SAND2018-10187

SANDIA REPORT

TBD
Unlimited Release
Printed September, 2018

Improve Replication of In-service Mechanical Environments

Tyler F. Schoenherr, Brett W. Clark, Pete Coffin

Prepared by
Sandia National Laboratories
Albuquerque, New Mexico 87185 and Livermore, California 94550

Sandia National Laboratories is a multimission laboratory managed and operated by National Technology and Engineering Solutions of Sandia, LLC., a wholly owned subsidiary of Honeywell International, Inc., for the U.S. Department of Energys National Nuclear Security Administration under contract DE-NA0003525.

Sandia National Laboratories

Issued by Sandia National Laboratories, operated for the United States Department of Energy by National Technology and Engineering Solutions of Sandia, LLC.

Available to DOE and DOE contractors from
U.S. Department of Energy
Office of Scientific and Technical Information
P.O. Box 62
Oak Ridge, TN 37831

Telephone: (865) 576-8401
Facsimile: (865) 576-5728
E-Mail: reports@adonis.osti.gov
Online ordering: http://www.osti.gov/bridge

Available to the public from
U.S. Department of Commerce
National Technical Information Service
5285 Port Royal Rd
Springfield, VA 22161

Telephone: (800) 553-6847
Facsimile: (703) 605-6900
E-Mail: orders@ntis.fedworld.gov
Online ordering: http://www.ntis.gov/help/ordermethods.asp?loc=7-4-0#online

TBD
Unlimited Release
Printed September, 2018

Improve Replication of In-service Mechanical Environments

Tyler F. Schoenherr

Abstract

Structural dynamic testing is a common method for determining if the design of a component of a system will mechanically fail when deployed into its field environment. To satisfy the test's goal, the mechanical stresses must be replicated. Structural dynamic testing is commonly executed on a shaker table or a shock apparatus such as a drop table or a resonant plate. These apparatus impart a force or load on the component through a test fixture that connects the unit under test to the apparatus. Because the test fixture is directly connected to the unit under test, the fixture modifies the structural dynamics of the system, thus varying the locations and relative levels of stress on the unit under test. This may lead to a false positive or negative indication if the unit under test will fail in its field environment depending on the environment and the test fixture. This body of research utilizes topology optimization using the Plato software to design a test fixture that attaches to the unit under test that matches the dynamic impedance of the next level of assembly. The optimization's objective function is the difference between the field configuration and the laboratory configuration's frequency response functions. It was found that this objective function had many local minima and posed difficulties in converging to an acceptable solution. A case study is presented that uses this objective function and although the results are not perfect, they are quantifiably better than the current method of using a sufficiently stiff fixture.

Acknowledgment

All bodies of research include several individuals in order to make progress. The research presented in this report is no different. The first acknowledgement goes to the L2 Milestone committee for this research. The committee provided critical feedback on the progress and results of this research periodically throughout the year. This feedback aided in providing direction to the Milestone. In no particular order, the committee consisted of Lili Heitman, John Pott, Laura Jacobs, Mike Ross, Denis Ridzal, Timothy Walsh. Also providing critical feedback was Ron Hopkins and Jerry Rouse in the work they did as external peer reviewers for this document.

Special thanks goes out to the Structural Testing Design Team. As a team, we met periodically throughout the year to discuss advances in test fixture design and trade ideas to advance the topic. The team included Julie Harvie, Mike Starr, Troy Skousen, Jacquelyn Moore, Dan Rohe, and Brandon Zwink. This team also includes David Soine and Richard Jones from the Kansas City Nuclear Security Complex. David and Richard participated in brainstorming sessions and collaboration involving topology strategies with respect to Frequency Response Function optimization within the Optistruct software.

Last, the Plato team deserves a lot of credit for the progress they made on the Plato software and the flexibility they demonstrated as the scope of what was needed changed throughout the year. This team was lead by Brett Clark and Pete Coffin. Not only did they provide the tools to make this milestone possible, they vehemently participated in finding methods to design vibration test fixtures. Their work directly lead to the success of this milestone.

Contents

List of Figures

List of Tables

Nomenclature

Field Configuration The setting where the designed hardware is in its designed assembled state

Field Environment The external force(s) imparted on the design configuration while the field configuration is in its designed use and the corresponding response by the field configuration

Component The hardware or subsystem of interest within the field configuration that needs to be tested prior to release into its field environment

Laboratory Environment The setting where the component is imparted by a controlled, prescribed force to cause a desired response of the component

Next level of assembly The structure to which the component is connected in its field configuration

Test fixture The piece of hardware to which the component is connected in its laboratory configuration

Frequency Response Function The Frequency Response Function (FRF) is a ratio between a motion response (i.e. displacement or acceleration) and the forcing function that caused it.

Chapter 1

Introduction

Many of Sandia's components and systems experience a vibration or shock environment that can cause structural damage or failure. To make the assertion that our systems meet their requirements, Sandia must qualify our components and systems to all environments they will experience, including vibration and shock environments. Testing a full system in all field shock and vibration environments to determine if it functions as intended is one method of qualification, however, this method is impractical in that it would be cost and time prohibitive and several iterations of testing would have to be done during the design of the system.

Instead of testing the entire system, individual components and subsystems are tested in a laboratory in a way that represents the environment that they would experience in the assembled system. The laboratory test requires a derived input function from an exciter such as a shaker table and a method of connecting the component or subsystem to the exciter in the form of a test fixture. The test fixture is critical because it changes the mode shapes and, therefore, possible stress states of the system. Figure 1.1 shows a flow chart of the two dynamic systems and the goal of producing the same stresses in the laboratory as was experienced in the field. If the stresses are not the same or bounded in the laboratory test, then the laboratory test will not necessarily exercise the same failure modes of the component or subsystem under test. If the laboratory test causes too high of stresses or stresses in the wrong location, then the test could produce a false failure mode. If the test does not excite the same failure modes, then the test fails its purpose.

The history of methods and means of performing structural dynamic tests range back to World War II [2]. Shaker devices used sinusoid outputs to test the equipment that was failing on naval ships during shocks from battle. This era also brought the development of the Shock Response Spectrum. It was not until the 1960s that environmental testing became more critical with respect to mission risk and some individuals began to recognize the impedance mismatch between the field configuration and laboratory configuration. The decades since brought several strategies for tailoring the input spectrum such as force limiting and multi-input control as methods of addressing some of the symptoms of impedance mismatch.

Through all the research and advancements, the guidelines for connecting the test article or unit under test to the shaker table or shock apparatus via a test fixture remain the same. Test fixture design guidelines state that the test fixture's first elastic natural frequency

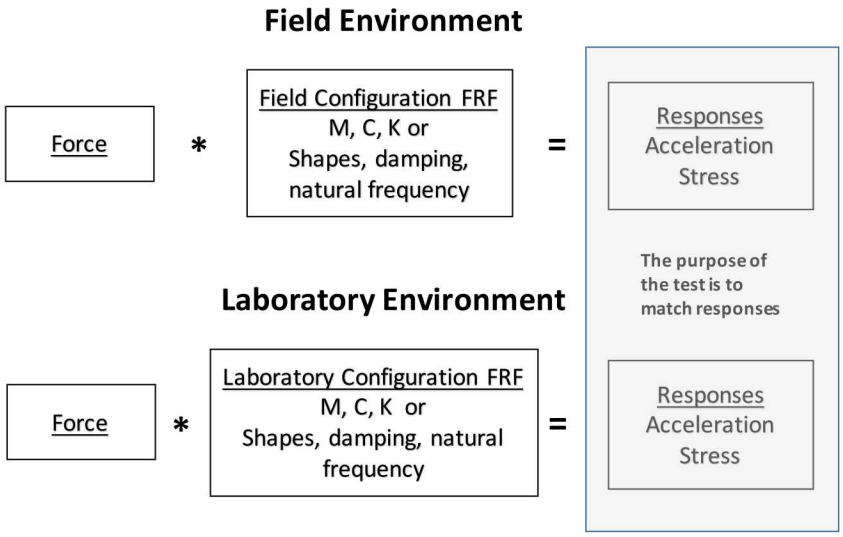

Figure 1.1: Flow chart highlighting the structure and goal of a structural dynamic laboratory test.

should be outside the range of the testing frequency. Although the rigid test fixture design ensures a constant transfer function from the source forcing function to the unit under test, it potentially modifies the laboratory configuration's frequency response functions with respect to the field configuration's frequency response functions. If the frequency response functions change, the mode shapes between the two configurations most likely will not remain the same and, therefore, the stresses cannot be the same.

Figure 1.2 is a layout of how the inputs for components are derived and tested today. The top row of Figure 1.2 shows a measurement taken at the base of the component. This measurement or base excitation is replicated in the laboratory environment on a rigid fixture. The bottom row of Figure 1.2 shows the displacement of the component in its field configuration. Because its connection points do not fall on a plane, the rigid fixture cannot replicate this stress state because all of the connection points stay on the same plane due to the fixture being rigid.

Topology optimization is a proposed method for designing a test fixture. Topology optimization is a finite element based method that either modifies the mesh or density of the elements to provide an optimized design based on a given objective function. Topology optimization is the basis for the research presented in this report. The goal of this research is to improve the fidelity of in-service component environments simulation through topology optimization. This research's focus is on the tools and prospective processes of developing a test fixture and not necessarily the implementation in today's qualification procedures. This research can be accurately described as a feasibility study.

This research supports a DOE Level 2 milestone objective. The completion or success

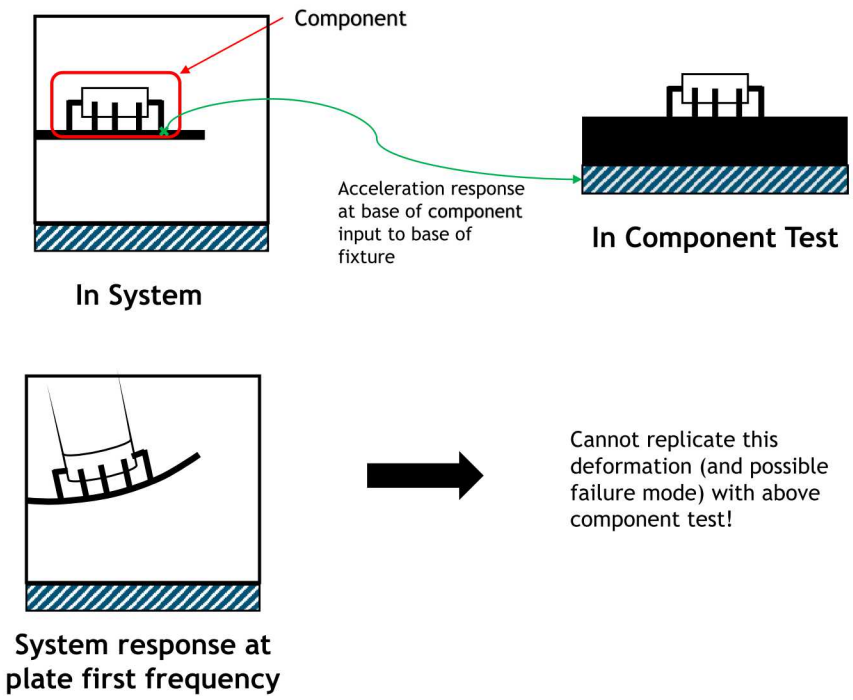

Figure 1.2: Example process of testing components in the laboratory.

criteria for this research is the following: Design a test fixture providing improved replication of mechanical environments will be designed using PLATO topology optimization for a test bed component. Using SIERRA finite element analysis, evaluate the component using (1) the test bed assembly, (2) a rigid fixture, and (3) the optimally made test fixture. The optimally made fixture must provide an improvement over the rigid fixture when compared to the test bed assembly.

This report gives an overview of the physics of the structural dynamics with respect to component and fixture interaction. It then provides an overview of topology optimization along with several strategies of implementing the tool to design a test fixture. It covers the examination of using the laboratory configuration's frequency response functions compared to the field configuration's frequency response functions as the objective function of the optimization problem.

This report then introduces a case study for which a test fixture is designed using topology optimization. The optimized fixture's performance with respect to stress is compared to a rigid fixture's performance. The result of this comparison shows that the optimization fixture provides an improvement to the stress levels when compared to the truth stresses, but not identical stresses. The results also show that optimization using the frequency response functions prove to be problematic due to the objective function containing numerous local minima.

The report concludes by examining other metrics and methods proposed during the research and their effects on the effort toward the design and utilization of test fixtures for

structural environmental testing. A metric was developed during this research that calculates the error that the test fixture introduces to the system in modal space to determine how the structure changed from its field configuration to its laboratory configuration. Another objective function is proposed in lieu of the frequency response function match. This objective function would be to match the Craig-Bampton constraint modes between the field and laboratory configurations. This would encompass the structure's mode shape space while optimizing on static solutions instead of dynamic solutions.

Chapter 2

Theory and Background

As stated in the Introduction, the goal of the laboratory test is to induce the same stresses on the component in the laboratory that the component experiences in the field. To determine if the laboratory test is successful, a method of experimentally determining stress is needed. Experimental stress is a difficult parameter to measure, but it is known that stress is proportional to strain for linear elastic materials through the elastic modulus shown as

$$\sigma_{xx} = E\epsilon_{xx} \tag{2.1}$$

where σ_{xx} is the stress in the x direction, E is the elastic modulus in the x direction, and ϵ_{xx} is the strain in the x direction. This relationship can be expanded to include three dimensional stress and strain. Strain is defined as the derivative of displacement with respect to its location shown as

$$\epsilon_{xx} = \frac{du}{dx} \tag{2.2}$$

where u is the x component of the displacement of a point with respect to its x coordinate.

From equations 2.1 and 2.2, it can be stated that if the displacement or motion of the component under test is the same in the field as in the laboratory, then the stresses in both configurations are the same.

To further enhance our understanding between the dynamics of a structure and its resulting displacement, one can transform the motion of an object to a linear combination of its eigenvectors or mode shapes. This transformation is written as

$$\bar{u} = \sum_{m=1}^{\infty} \boldsymbol{\phi_m} q_m \tag{2.3}$$

where $\boldsymbol{\phi_m}$ are the mode shapes, q_m are the modal coordinates of mode m, and $\bar{u}$ is the vector of displacements for the degrees of freedom.

Displacement can be viewed in the physical domain, the frequency domain, or the modal

domain. If the motion is examined in the frequency domain in the form of frequency response functions (FRFs), then the mode shapes are the imaginary parts at the component's natural frequencies as shown in Figure 2.1. Figure 2.1 also shows that a given set of FRFs at degrees of freedom that uniquely describe the mode shape with respect to the other mode shapes in the given space are enough to identify the motion of the entire component.

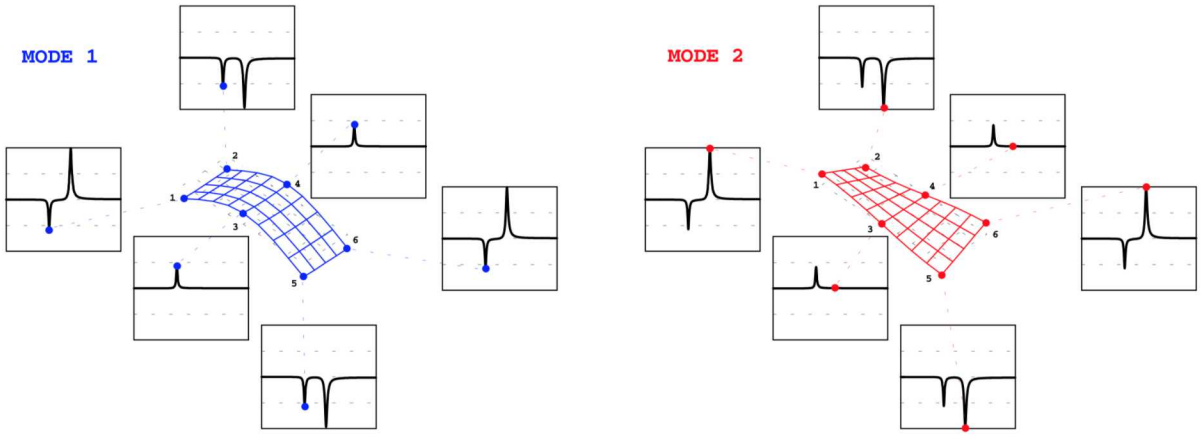

Figure 2.1: Mode shapes of a plate calculated from the imaginary part of the FRF [1]

The work presented in this report is focused on creating a test fixture that matches the same impedance as the next level of assembly in the field configuration. This matching impedance is viewed in this report as having the same FRFs in both configurations. Throughout this report, matching the FRF is the objective, however, it is seen in this section that multiple FRFs must match in order to ensure that the mode shape at the appropriate natural frequency matches in the field and laboratory configurations. The number of FRFs needed to match is equal to the number of modes needed to be matched. The response degrees of freedom of the FRFs must also make the mode shapes independent. This is to all ensure that the correct shape is being excited which enforces the correct stresses.

Equations 2.1 through 2.3 show that the linear combination of the mode shapes of the component or unit under test dictate the component's stresses. To enhance the insight on the sources of error between the flight configuration and the laboratory configuration, the component's mode shapes are transformed into Craig-Bampton space. Craig-Bampton space states that the system's mode shapes can be transformed into its fixed base mode shapes and Craig-Bampton constraint shapes. An example of these shapes is shown in Figure 2.2.

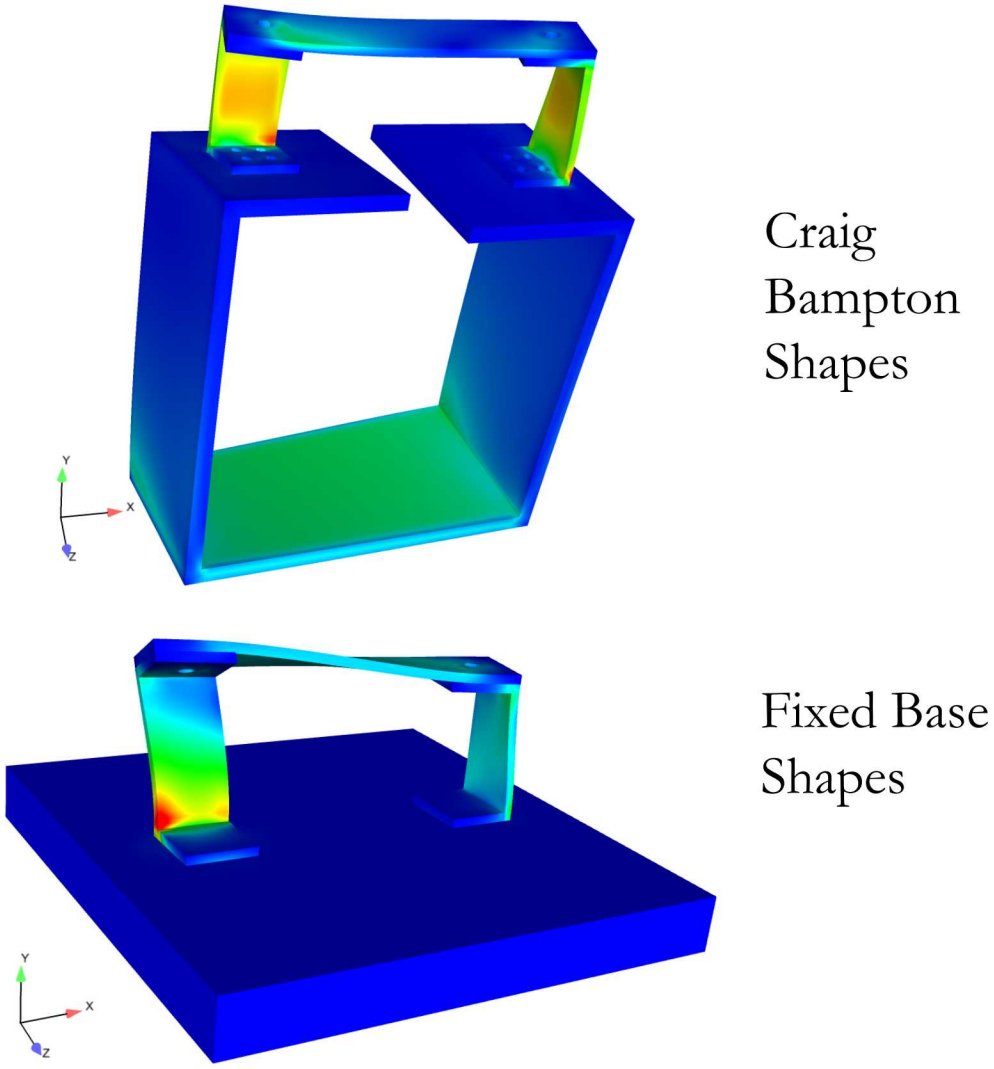

Figure 2.2: Visual of a component's motion in Craig-Bampton space, a linear combination of fixed base modes and Craig-Bampton constraint modes. Color plot is relative stress.

Chapter 3

PLATO Development

In support of this milestone, various new capabilities were developed in the PLATO topology optimization product. This section describes these new capabilities, illustrates the magnitude of work that was accomplished and new capabilities in PLATO that resulted from the milestone. Much of this development was driven by experience using commercial topology optimization packages.

FRF Matching using Density Approach

Prior to the beginning of the milestone effort, PLATO did not have any capabilities for matching FRFs or utilizing Levelset methods. The initial development focused on a density-based capability. The density-based approach was easy/quick to implement while leveraging existing Sierra/SD inverse methods FRF capabilities and allowed the analysts to start running problems early in the milestone cycle while the levelset approach was being developed. However, based on experience with commercial packages, the density-based approach would ultimately not be sufficient and a levelset-based approach would be needed to more accurately model the physics. Developing the density-based approach provided foundational capabilities and frameworks that would be reused in the levelset approach so the effort was not wasted. Furthermore, it provided the ability to make comparisons with commercial packages.

FRF Matching using the Levelset Method

A critical feature of the levelset method is that an explicit representation of the material boundaries (and geometry) are constructed from design variables. At each design iteration, the response is computed using a finite element representation that abides by this geometry. In density methods the geometry is smeared on the finite element mesh. Elements on the boundary between materials are represented as a mixture between materials or material and void, that is, density of intermediate value. If significant regions of intermediate value exist, the finite element calculation of response is not an accurate representation of the discrete material, material a, b, or void. Deterrence of intermediate densities is a function

of the optimization problem formulation. As described elsewhere in this report, early testing indicated that intermediate densities were not deterred by naive density method formulations. Solid Isotropic Microstructure with Penalization (SIMP) was used here. Due to this, using a levelset method, which does not suffer from this complication, was seen as an appealing alternative and became the focus of the efforts. In the rest of this section we will discuss the formulation and implementational details of the levelset FRF matching method that was added to PLATO for this milestone.

Problem Definition

The PLATO development work was completed with the goal of solving an optimization problem defined as:

$$\begin{array}{ll} \underset{\mathbf{s}}{\text{minimize}} & J(\bar{\mathbf{u}}, \mathbf{p}) \\ \text{subject to} & \mathbf{R}(\bar{\mathbf{u}}_{km}, \mathbf{p}, \bar{\mathbf{f}}_m, \omega_k) = \mathbf{0}, \\ & g_i \leq 0, \\ \textit{where} & k = 1, \ldots, N_{freq}, \\ & m = 1, \ldots, N_{loads}, \\ & i = 1, \ldots, N_{constraints}. \end{array} \tag{3.1}$$

Here we seek to minimize an objective $J(\bar{\mathbf{u}}_{km}, \mathbf{p})$ that is a function of the Fourier Transform of the displacements $\bar{\mathbf{u}}_{km}$ at frequency ω_k and for load m. This is subject to a set of constraints (that we will leave undefined for the moment) g_i and to the solution of the discretized Frequency Response Function (FRF) equation $\mathbf{R}(\bar{\mathbf{u}}_{km}, \mathbf{p}, \bar{\mathbf{f}}_m, \omega_k)$, a function of the states, design variables $\mathbf{p}$, Fourier transformed loads $\bar{\mathbf{f}}_m$ and frequency ω_k.

The governing equations ($\mathbf{R}$) of the FRF can be written as:

$$\mathbf{R}(\bar{\mathbf{u}}_{km}, \mathbf{p}, \bar{\mathbf{f}}_m, \omega_k) = (\mathbf{K} + i\ \omega_k\ \mathbf{C} - \omega_k^2\ \mathbf{M})\ \bar{\mathbf{u}}_{km} - \bar{\mathbf{f}}_m, \tag{3.2}$$

where the mass $\mathbf{M}$, stiffness $\mathbf{K}$ and damping $\mathbf{C}$ matrices may all be functions of the design variables $\mathbf{p}$. This is equivalent to Equations (19) and (30) in [4].

Sensitivities

We will consider reduced-space optimization methods where the optimization algorithm requires the following expressions:

- The objectives
- The constraints
- Derivatives (sensitivities) of the objective with respect to the design variables

- Derivatives of the constraints with respect to the design variables.

In this section, we will show the calculation of the derivatives of a generic function $Z(\bar{\mathbf{u}}_{km}, \mathbf{p})$ with respect to the design variables. We will use Z here to highlight that the derivation is applicable to either objectives or constraints which are functions of the states resulting from the FRF solution case.

The total derivative of the criteria Z can be written as:

$$\frac{dZ}{d\mathbf{p}} = \frac{\partial Z}{\partial \mathbf{p}} + \sum_{k=1}^{N_{freq}} \left\{ \sum_{m=1}^{N_{loads}} \left(\frac{\partial Z}{\partial \bar{\mathbf{u}}_{km}} \frac{\partial \bar{\mathbf{u}}_{km}}{\partial \mathbf{p}} \right) \right\}, \tag{3.3}$$

where

$$\frac{\partial Z}{\partial \bar{\mathbf{u}}_{km}} \frac{\partial \bar{\mathbf{u}}_{km}}{\partial \mathbf{p}} = \frac{\partial Z}{\partial \bar{\mathbf{u}}_{km}} \left[\frac{\partial \mathbf{R}_{km}}{\partial \bar{\mathbf{u}}_{km}} \right]^{-1} \frac{\partial \mathbf{R}_{km}}{\partial \mathbf{p}}. \tag{3.4}$$

We can compute the adjoint solution λ_{km}:

$$\left[\frac{\partial \mathbf{R}_{km}}{\partial \bar{\mathbf{u}}_{km}} \right] \lambda_{km} = - \left[\frac{\partial Z}{\partial \bar{\mathbf{u}}_{km}} \right]^{T}, \tag{3.5}$$

so we can write the total derivative as:

$$\frac{dZ}{d\mathbf{p}} = \frac{\partial Z}{\partial \mathbf{p}} + \sum_{k=1}^{N_{freq}} \left\{ \sum_{m=1}^{N_{loads}} \left(\lambda_{km} \frac{\partial \mathbf{R}_{km}}{\partial \mathbf{p}} \right) \right\}. \tag{3.6}$$

Equation 3.5 can be seen as (20) in [4] while Equation 3.6 is (21) in the same work.

Direct Derivative

In this section we discuss the details of computing the direct, partial derivative of the criteria with respect to the design variables:

$$\frac{\partial Z}{\partial \mathbf{p}}. \tag{3.7}$$

Given the current driver, matching FRFs at nodes, it is expected that Equation 3.7 will be zero.

State dependence

In this section, we discuss the details of computing the influence of the design variables on the criteria, Z, via their influence on the state variables. This is:

$$\sum_{k=1}^{N_{freq}} \left\{ \sum_{m=1}^{N_{loads}} \left(\frac{\partial Z}{\partial \bar{\mathbf{u}}_{km}} \frac{\partial \bar{\mathbf{u}}_{km}}{\partial \mathbf{p}} \right) \right\} \tag{3.8}$$

or written using the adjoint,

$$\sum_{k=1}^{N_{freq}} \left\{ \sum_{m=1}^{N_{loads}} \left(\lambda_{km} \frac{\partial \mathbf{R}_{km}}{\partial \mathbf{p}} \right) \right\}. \tag{3.9}$$

From Equation 3.9, it is observed that there will be an adjoint solve (and corresponding adjoint vector λ_{km}) for each load and frequency step. Given that many frequency steps are likely necessary to achieve a good fit, this may indicate that it would be worth studying the relative computational cost of performing topology optimization with modal methods for FRFs.

As with common elasticity optimization problems, the adjoint calculation requires the objective function gradient with respect to the states and the derivative of the residual with respect to the states (frequently required by Newton solvers for the forward problem). The second part of Equation 3.9 is the derivative fo the residual with respect to the design variables, $\frac{\partial \mathbf{R}_{km}}{\partial \mathbf{p}}$, the calculation of which may have different implications based on the form of the geometry definition (level-set, density method, etc).

In topology optimization, the full matrix form of $\frac{\partial \mathbf{R}_{km}}{\partial \mathbf{p}}$ is not constructed. Rather, the element-wise product with the adjoint is assembled into the gradient vector.

$$\sum_{k=1}^{N_{freq}} \left\{ \sum_{m=1}^{N_{loads}} \left(\lambda_{km} \frac{\partial \mathbf{R}_{km}}{\partial \mathbf{p}} \right) \right\} = \sum_{k=1}^{N_{freq}} \left\{ \sum_{m=1}^{N_{loads}} \left(\sum_{j=1}^{N_{elem}} \left[\lambda_{kmj} \frac{\partial \mathbf{R}_{kmj}}{\partial \mathbf{p}} \right] \right) \right\}, \tag{3.10}$$

where $\mathbf{R}_{kmj}$ and λ_{kmj} are the gradient and adjoint existing on the degrees of freedom for a given element j. For current use cases where the load is not changing with the design geometry the adjoint will be constant across all loads, that is that:

$$\lambda_{k1} = \lambda_{k2} = \ldots = \lambda_{kN_{loads}}. \tag{3.11}$$

For density methods (such as SIMP), the gradient of the element residual with respect to the design variables can typically be computed analytically. For SIMP, the material properties may be interpolated as:

$$E = E_0 \ \rho_f^{p_p}, \tag{3.12}$$

where the element elastic modulus E is a function of the material elastic modulus E_0, the fictitious density ρ_f and a penalty parameter p_p. The resulting stiffness matrix gradient can be computed as:

$$\frac{\partial \mathbf{K}_e}{\partial \mathbf{p}} = \frac{\partial \rho_f}{\partial \mathbf{p}} \left[p_p \ \rho_f^{p_p - 1} \ \int_{\Omega_e} \left(\mathbf{B}^T \ \mathbf{D}(E_0) \ \mathbf{B} \right) d\Omega_e \right], \tag{3.13}$$

where the standard element constitutive matrix $\mathbf{D}$ is computed using the material elastic modulus E_0 and the normal deformation gradients $\mathbf{B}$.

For the eXtended Finite Element Method (XFEM) or Conformal Decomposition Finite Element Method (CDFEM) we would expect to compute the element residual gradients

partially by finite difference. The current work utilizes CDFEM in Sierra/SD, the finite difference would be computed on node coordinate position. The resulting form would appear as:

$$\frac{\partial \mathbf{R_{km}}}{\partial \mathbf{p}} = \frac{\partial \mathbf{R_{km}}}{\partial x_{ij}} \frac{\partial x_{ij}}{\partial \mathbf{p}}, \tag{3.14}$$

where x_{ij} is the j-th coordinate of node i. $\frac{\partial \mathbf{R_{km}}}{\partial x_{ij}}$ having been computed by finite difference and $\frac{\partial x_{ij}}{\partial \mathbf{p}}$ having been computed by the geometry engine that provides the element decomposition. The geometry engine that provides the changing finite element discretization is the XFEM Toolkit (XTK).

The PLATO team has a research contract with the University of Colorado in Boulder, who are developing XTK. XTK is a library for generating a conformal mesh using XFEM (eXtended Finite Element Method) techniques given a background mesh and a levelset field. Along with the conformal mesh, XTK also outputs sensitivities of the geometry with respect to changing the levelset values on the background mesh. The XTK library is an essential part to providing a levelset-based topology optimization capability. The development of the XTK library reached maturity during the milestone cycle and was utilized in the levelset-based capability.

Objective Function J Details

In this section, we will discuss the objective functions that were considered during this milestone. These are FRF mismatch or error measures. The baseline FRF error measure from [4] is:

$$J_{FRF}(\bar{\mathbf{u}}, \mathbf{p}) = \sum_{k=1}^{N_{freq}} \left\{ \sum_{m=1}^{N_{loads}} \left(\sum_{i=1}^{N_{match\_dof}} \left[\frac{(\bar{u}^i_{ikm} - \bar{\bar{u}}^i_{ikm})^2}{A_{ikm}} + \frac{(\bar{u}^R_{ikm} - \bar{\bar{u}}^R_{ikm})^2}{A_{ikm}} \right] \right) \right\}, \tag{3.15}$$

where the normalization term A_{ikm} is based on the largest response at a given frequency. That is:

$$A_{km} = max_i \left(|\bar{u}_{ikm}| \right). \tag{3.16}$$

The objective is a function of the reference response $\bar{\bar{u}}_{ikm}$ and the current response $\bar{u}_{ikm}$ where superscript i indicates the imaginary component and superscript R the real part. In 3.15 we highlight that the objective will seek to match the FRF for a particular set of degrees of freedom (DOFs). For the current proposed use case this means all DOFs of a user-selected subset of finite element nodes. The selected set of nodes will generally be small in number, fewer than 1000.

The second and third objective formulations are simple variations on the first, where only the real:

$$J_{FRF}(\bar{\mathbf{u}}, \mathbf{p}) = \sum_{k=1}^{N_{freq}} \left\{ \sum_{m=1}^{N_{loads}} \left(\sum_{i=1}^{N_{match\_dof}} \left[\frac{(\bar{u}^R_{ikm} - \bar{\bar{u}}^R_{ikm})^2}{A_{ikm}} \right] \right) \right\}, \tag{3.17}$$

or imaginary:

$$J_{FRF}(\bar{\mathbf{u}}, \mathbf{p}) = \sum_{k=1}^{N_{freq}} \left\{ \sum_{m=1}^{N_{loads}} \left(\sum_{i=1}^{N_{match\_dof}} \left[\frac{(\bar{u}^i_{ikm} - \bar{\tilde{u}}^i_{ikm})^2}{A_{ikm}} \right] \right) \right\}, \tag{3.18}$$

parts of the response are matched.

One may also only measure error in the magnitude of response, that is:

$$J_{FRF}(\bar{\mathbf{u}}, \mathbf{p}) = \sum_{k=1}^{N_{freq}} \left\{ \sum_{m=1}^{N_{loads}} \left(\sum_{i=1}^{N_{match\_dof}} \left[\frac{(|\bar{u}_{ikm}| - |\bar{\tilde{u}}_{ikm}|)^2}{A_{ikm}} \right] \right) \right\}. \tag{3.19}$$

Finally an error measure on the magnitude of response was constructed where the orthogonal or shortest distance between the current and reference response curves was measured. In the previous measures the error at each frequency line is the vertical distance between the responses. This orthogonal distance measure can be written as:

$$J_{FRF}(\bar{\mathbf{u}}, \mathbf{p}) = \sum_{k=1}^{N_{freq}} \frac{1}{C_k} \left\{ \left(min_j \left| \vec{B}^k - \vec{\tilde{B}}^j \right| \right)^2 \right\}, \tag{3.20}$$

where $\vec{B}^k$ is the vector constructed by the frequency and natural log of the response magnitude $[\omega_k, ln\left(|\bar{u}_{ikm}|\right)]$ at frequency ω_k while $\vec{\tilde{B}}^j$ is the vector corresponding to the reference response at frequency ω_j. C_k is a scaling coefficient, initially 1. This measure is the integration across frequency of the shortest distance between the natural log of the current and reference response curves.

Constraints and Regularizations

Surface Area Constraint and Gradient

In an effort to help regularize the objective function and make it more convex we implemented an optional surface area constraint (and corresponding gradient) or objective penalty. For some test problems this did aid in converging to sensible results but experience was necessary to determine an appropriate constraint value. The surface area was computed on the interface between the material and void in the design domain Γ_D, that is:

$$\int_{\Gamma_D} 1 \, d\Gamma. \tag{3.21}$$

Volume Penalty

Experience also indicated that volume is a useful geometric measure to penalize or constrain in topology optimization problems. The volume is simply:

$$\int 1 \; d\Omega, \tag{3.22}$$

which may be used as a penalty on the objective:

$$J(\bar{\mathbf{u}}, \mathbf{p}) = J_{FRF}(\bar{\mathbf{u}}, \mathbf{p}) + c_v \int 1 \; d\Omega, \tag{3.23}$$

where c_v is a scaling parameter or as a constraint as:

$$g = \frac{1}{V_c} \int 1 \; d\Omega \; - 1, \tag{3.24}$$

where V_c is the largest allowable volume.

Design Variable Filtering

The abstract set of design variables for the levelset method are nodal values of the levelset field defined on the background finite element mesh. The CDFEM decomposition is constructed from a levelset field that is the result of the application of a linear filter on the abstract design variable field. The linear filter is that of Bruns and Torterelli[**?**], a weighted distance measure.

Implementation Details and Features

Leveraging Sierra/SD Inverse Methods Framework

The Sierra/SD physics code contains capabilities for solving inverse problems using gradient-based techniques, the same type of techniques used to solve topology optimization problems. The inverse methods in Sierra/SD and topology optimization are similar in that they use gradient-based optimization methods to solve problems that are constructed from the output of a finite element method. Scalar objective functions are constructed from typical finite element quantities of interest: stress, strain and displacement, and the derivatives of these quantities must be calculated with respect to some optimization variables.

Topology optimization and inverse methods will almost always differ in the definition of optimization variables and will often differ in the definition of the objective function. In this

work the initial objective function for the FRF match was shared with an existing inverse methods capability, in Equation 3.4 this means that:

$$\frac{\partial Z}{\partial \bar{\mathbf{u}}_{km}} \left[\frac{\partial \mathbf{R}_{km}}{\partial \bar{\mathbf{u}}_{km}} \right]^{-1}, \tag{3.25}$$

is identical in the existing inverse methods capability and the initial topology optimization work. In an effort to not duplicate code and to save development time it was decided to directly use portions of the existing inverse methods framework for this topology optimization development. This meant that new objective function formulations were developed in the inverse methods framework and that an interface between the inverse methods framework and the topology optimization framework was developed for calculating partial derivatives with respect to design variables.

Recent work on the Plato Engine MPMD framework was used for this work so that the CDFEM decomposition was effectively a preprocessing step before each optimization iteration's analysis in Sierra/SD. Partial derivative information of interface node coordinates with respect to design variables was passed into Sierra/SD and used to complete the chain rule so that the complete derivative of quantities of interest could be returned with respect to the design variables. The interface linking the topology optimization framework to the inverse methods framework utilized constructs that allowed for generic design variable definitions, with the goal of minimizing code duplication between density and levelset methods.

Optimization Algorithms with Globalization Techniques

To provide a good opportunity for finding good solutions to the non-convex FRF matching problem, we implemented two additional optimization algorithms that included globalization methods to help avoid local minima in the solution space. These were the Globally Convergent Method of Moving Asymptotes (GCMMA) and the Kelley Sachs Bound Constrained (KSBC) algorithms. GCMMA requires a constraint as part of the problem formulation and KSBC does not. The need to be able to switch between optimization algorithms also required the implementation of an abstract interface to the optimization algorithm used in PLATO.

Levelset Initialization Methods

The levelset-based solution to a topology optimization problem is dependent on the initial values of the levelset field. Additionally, as opposed to density methods where a constant, intermediate density value may be used as the initial condition (imparting no particular geometry), the levelset method requires a meaningful initial geometry. Therefore, we developed a few different methods for initializing the levelset field. One method generates a levelset with a number of voids on the interior (a "swiss cheese" pattern) to give the optimizer a complex initial topology. Another method allows the user to start with a levelset field that is based on a simple parallel-piped primitive. The user can also select "surfaces" on

the background mesh that will be prescribed to be void in the initial levelset field, effectively placing a design interface next to this background mesh surface. These various methods allowed the analysts to run the problems needed for the milestone but there are certainly many other initialization methods that could be implemented and which would be useful.

Support for Tet10 Elements

It is common knowledge that 4-noded, tri-linear tetrahedral elements have poor accuracy with coarse meshes for structural dynamics problems. The use of 10-noded, higher-order tetrahedra was desired to allow for more accurate response estimation during the optimization process. The XTK developers implemented a capability that added mid-side nodes to the output CDFEM mesh. This capability was enabled in the PLATO software. Due to the nature of the CFEM implementation in Sierra/SD only a few very minor changes were necessary to support the new element type.

Restart Capability

One of the unique capabilities of previous versions of PLATO has been the ability to restart a topology optimization run from an intermediate or final design of a prior run. This can be useful when attempting continuation approaches where changing optimization problem parameters are desired during optimization process. Continuation approaches are frequently used to work-around problematic behavior in topology optimization problems. This capability had not been enabled in the newly architected version of PLATO where all of the FRF matching capabilities were being implemented. Therefore, the restart capability was implemented in the new version of PLATO so that it could be used when doing FRF matching runs.

Quantity of Interest Plotting

A Graphical User Interface (GUI) is a key feature of PLATO, allowing analysts to easily interact with their optimization problem and solutions. To support the FRF matching development, the ability to plot critical quantities of interest, like the FRF were added to the PLATO GUI.

Chapter 4

Designing a Dynamic Test Fixture using Topology Optimization

This chapter covers all of the topology optimization work done to explore the use of FRF matching as an objective function. The first section of this chapter documents the work done using topology optimization and matching frequency response functions (FRFs) in the Altair Optistruct software. Optistruct was explored because the software had the capability for FRF matching as an objective function and it was readily available when PLATO was developing its capabilities. The Optistruct runs framed the problem space and explored the general difficulties of designing a test fixture with the FRF matching objective function.

The second section covered the optimization work done by the PLATO software. It explored some of the effects of choosing different strategies for defining error and other design parameters within the optimization space. This section also defined the final test bed and analysis that satisfied the success criteria of the level 2 milestone.

Topology Optimization using Optistruct

Although the milestone for this report dictated that the PLATO software must be used, it was determined in the onset of this research that an alternate software should be examined for comparison of usability and results. Also, PLATO did not have the FRF matching capability at the beginning of the research so the Optistruct runs were able to aid in the design direction of the PLATO software.

The work presented in this section used the density method for topology optimization. The hardware used as the test bed in this section was the Box Assembly with Removable Component (BARC) hardware and is shown in Figure 4.1. The BARC hardware was designed to be a challenge problem for the structural dynamics community with the intent of developing methods of designing test fixtures. In relation to the problem description laid out in the Introduction section in Chapter 1, the blue block box assembly was the next level of assembly and the red removable component was the component or unit under test. Figure 4.1 shows the field configuration.

To set up the optimization analysis, the fixed space and the design space had to be

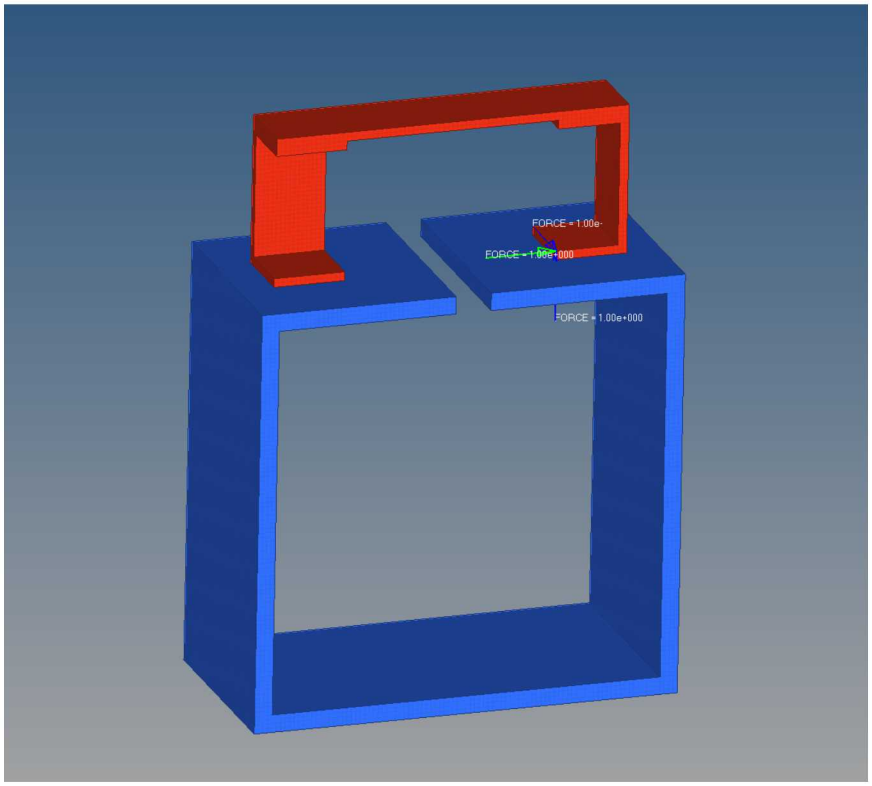

Figure 4.1: Finite element model of the BARC system with the blue block being the box assembly and the red block being the removable component. This is the field configuration for the BARC.

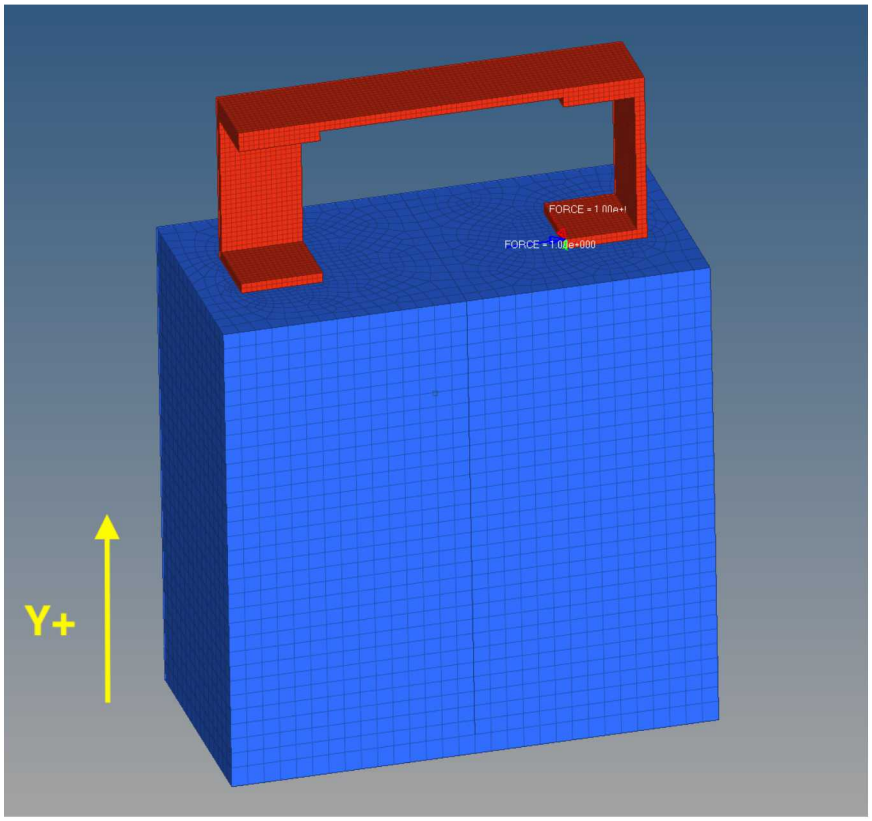

Figure 4.2: Finite element model of the removable component in red attached to the design space in blue.

identified. The removable component was designated to be fixed space which meant that the optimizer could not change its density or form. The removable component was attached to a block which was the optimization space. In the density method, the optimization space was the region where the elements' density was allowed to vary between 0 and 1 with 0 being non-existent and 1 being fully present. This initial optimization configuration is shown in Figure 4.2.

Initial runs of the optimization problem using the FRF matching objective function in Equation 3.15 showed no or small changes to the error of the objective function and that the solution had converged. This was problematic because the field and laboratory frequency response functions chosen were barely improved upon visual inspection. An example of these plots are shown in Figure 4.3. The lack of change in the topology design implied that the initial condition was close to a local minima to which the solution converged. Different aspects of the optimization problem were modified to determine if better results could be obtained. Parameters changed were the amount of FRFs used, the frequencies of only around the natural frequencies, convergence rates, SIMP penalty factor, and using the imaginary part of the FRF in the error calculation.

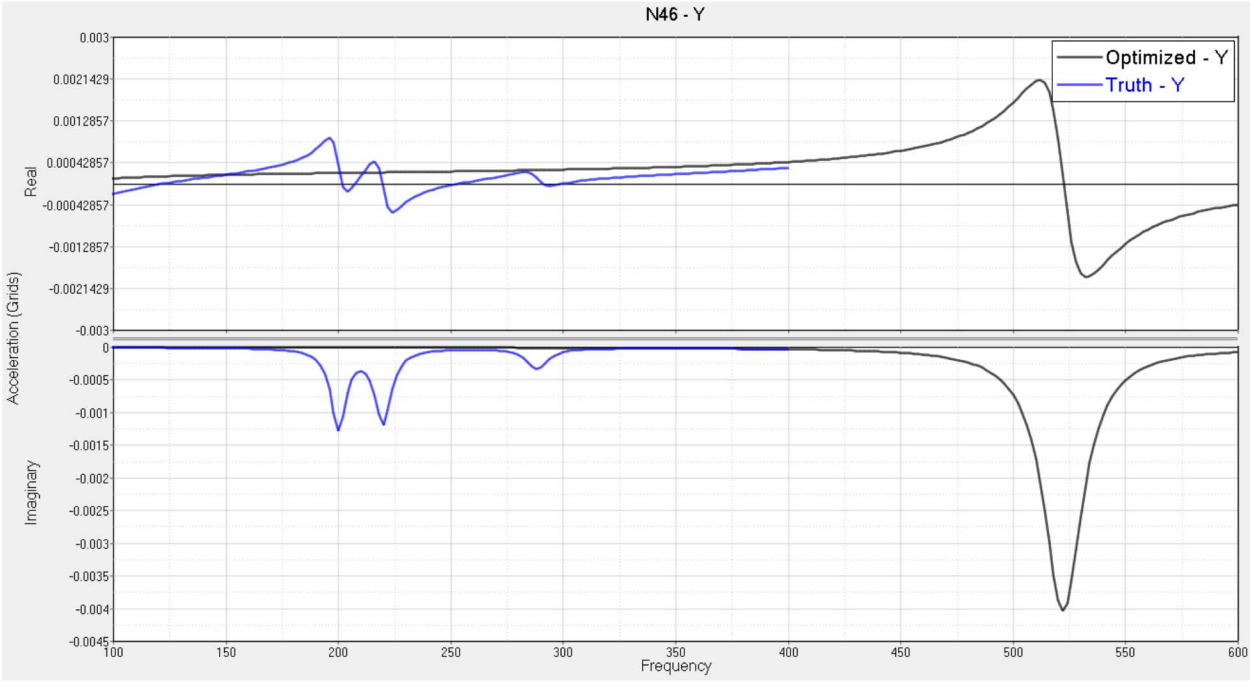

Figure 4.3: Example of an unacceptable local minima in a FRF matching optimization run. Truth is the field configuration and Optimized is the converged solution.

Many runs showed that the many local minima in the optimization space were an issue in matching frequency response functions. A contrived error from the FRF matching objective function was created to illustrate these local minima in Figure 4.4. With no active means to locate the global minima verses a local minima, it was of interest to create a test to determine how close the initial condition needed to start to the global minima to find it.

The designed test to determine how close the initial condition had to be to the global minima used the BARC system previously identified. The setup used the field configuration's geometry as the initial geometry for the optimization. This would make the global minima solution a density of 1 for all of the elements in the optimization space since the geometry of the design space was the same as the field configuration.

The initial condition was changed by altering the initial density for the elements. Seven runs with different initial densities were run. These runs and their results are documented in Table 4.1. The FRFs for Runs 3 and 4 were plotted in Figure 4.5. There were two conclusions from this series. The first was that to converge to the global minima, the initial condition needed to be relatively close to the global minima as to not get stuck in a local minima. The second conclusion was that there exists some (not all) parameters that alter the objective function's error space that reduce the number of local minima.

Several other runs were executed in Optistruct with no improvement on the matching of the frequency response function matching. Each run would quickly converge to a local minima. It was observed on some of these runs that the higher order modes would be altered so that their residuals would become an average line through the target frequency response

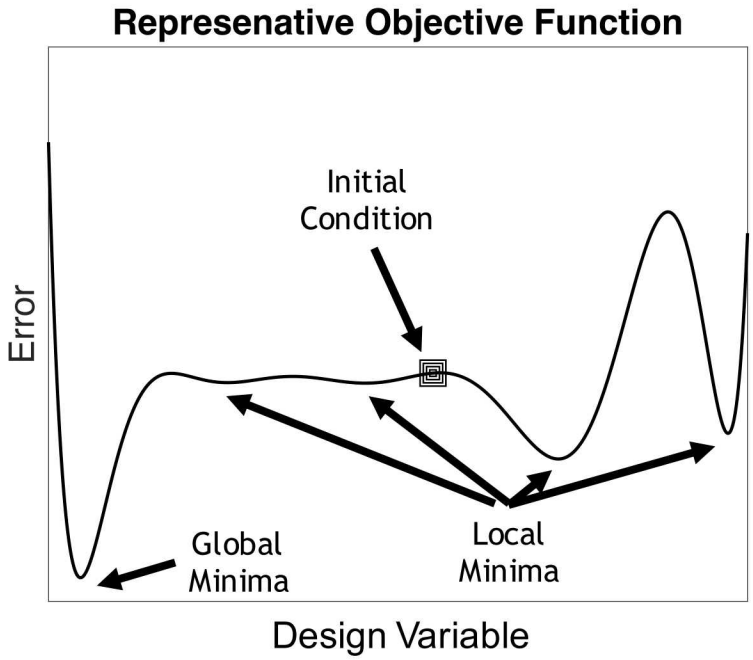

Figure 4.4: Contrived error plot for a FRF matching objective function.

Table 4.1: Results of topology optimization trivial solution on BARC hardware

Run #	Initial Density	Result
1	1.0	The densities did not change
2	0.9	Almost all of the densities converged to 1.
3	0.8	The densities did not converge to 1 but converged to overall different system dynamics
4	0.8	The SIMP penalty factor was changed from 3 to 1. The densities converged to 1 in a single iteration.
5	0.5	Left the SIMP penalty factor at 1. The derivatives were 0 and the densities never changed.
6	0.5	Expanded the frequency range from (196 Hz-292 Hz) to (20 Hz-1000 Hz) and the results did not change.
7	0.5	Changed the SIMP penalty factor from 1 to 1.2. The densities of all elements converged to 0.95.

function.

Figure 4.6 shows a topology run with the target or truth data, the initial topology optimization model, and the final optimized model. In the figure, one can see that a natural frequency of the optimized model converged to one of the natural frequencies of the target data at approximately 200 Hz. However, the source of most of the error calculated came from the higher frequencies. The optimizer found a local minima that increased the acceleration

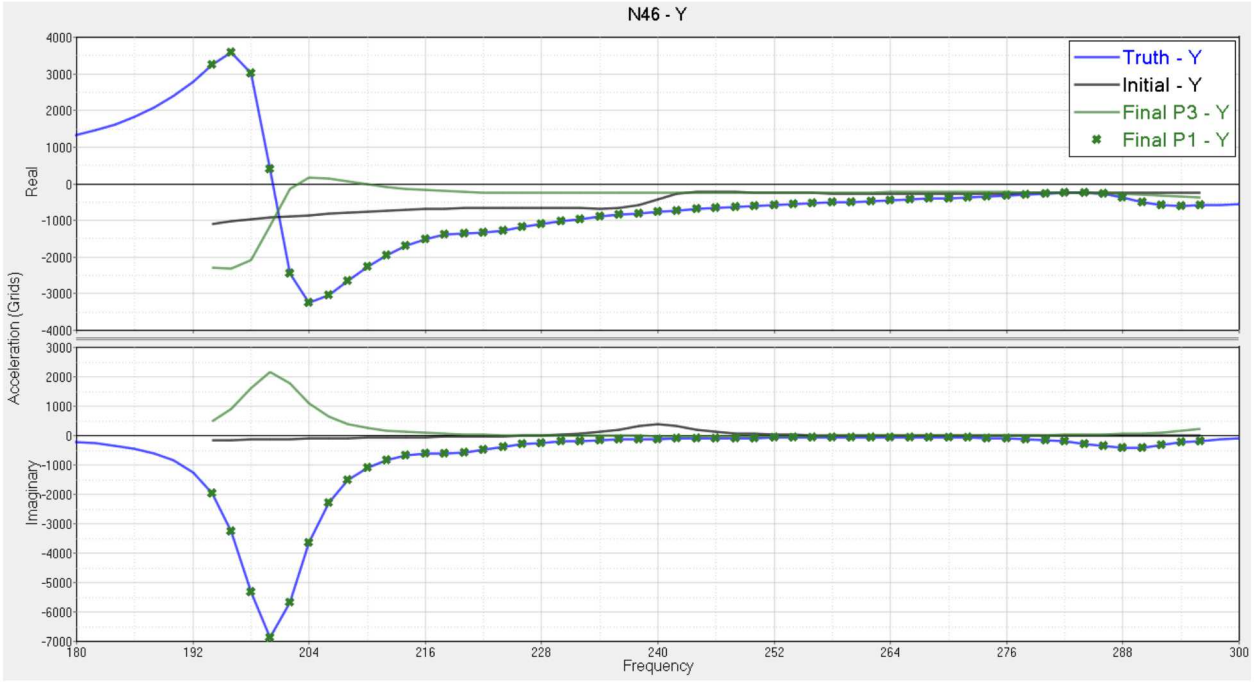

Figure 4.5: Frequency Response Functions of optimization solution with initial density of 0.8. Run 3 is the solid green line and Run 4 is the green (x) marks

response at a natural frequency at approximately 15 kHz so that its residual crossed the target data in the frequency range between 1200 Hz and 2000 Hz. This use of the residuals of higher modes demonstrated how the design space of the optimization problem can change so that a local minimum is quickly found.

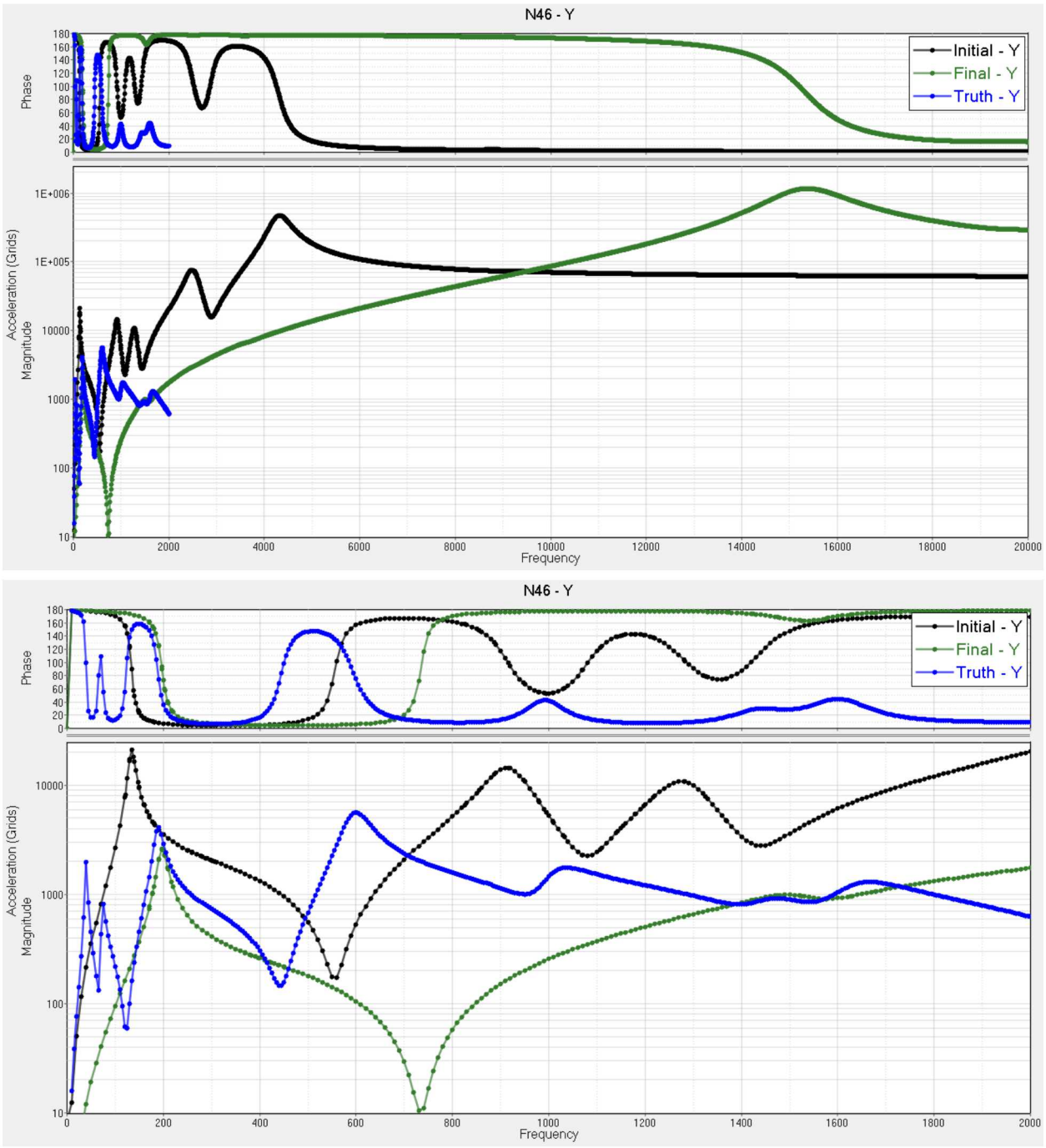

Figure 4.6: Example of the optimization solution modifying out of band modes to modify the mode's residuals to optimize the FRF match objective function.

Topology Optimization using PLATO

Through this research, the PLATO software was enhanced to include a new objective function for matching the Frequency Response Functions (FRF) of selected degrees of freedom on an optimization finite element model to a target finite element model's FRFs. This objective function was the same as was run in the Optistruct software. During the course of the year, several enhancements were made to the PLATO software. These enhancements included the implementation of levelset optimization, including higher order tet-10 elements, and the restart capability so that continuation optimization would be an option.

Optimization runs using Optistruct demonstrated that optimizing on matching FRFs between two systems is a very difficult problem due to the many local minima that exist in the error space of the solution. It would be advantageous to examine the error space of this optimization problem to learn about the sources and locations of the local minima, however, the error space for a topology optimization problem has thousands of variables which make it impossible for the analyst to examine. Due to the difficulty of examining the error space of a full topology optimization problem, a simple cantilever beam example was developed.

Comparison of FRF Match Measures

A simple cantilever beam is used to demonstrate the differences between the FRF match measures. The beam is 40 units in length, 1 in width and has a thickness varying between 0.05 and 0.5. A force along the free end is applied that has a constant magnitude in frequency. The displacement response is measured at the end of the beam. The value of thickness equal to 0.2 is chosen as the reference thickness, the 'truth' value. We evaluated a frequency range from 0 to 100 Hz, which captures three modes in the reference configuration.

Figure 4.7 shows a comparison of the FRF match measures (Equations 3.15, 3.19, 3.17, 3.18 and 3.20 respectively) as the thickness varies. They are plotted here on a log scale due to the large range of residual values of the different measures. All of the measures show numerous local minima while the cluster of measures surrounding the 'baseline' measure show very significant oscillation for small beam thicknesses. Plotting the measures on a linear scale and zooming in, Figure 4.8, we see that nearly all of the measures also tail-off for larger beam thicknesses. For this problem in particular it seems that the Log-Magnitude Measure, produces the most non-oscillatory path to the global minima (closest to a convex objective).

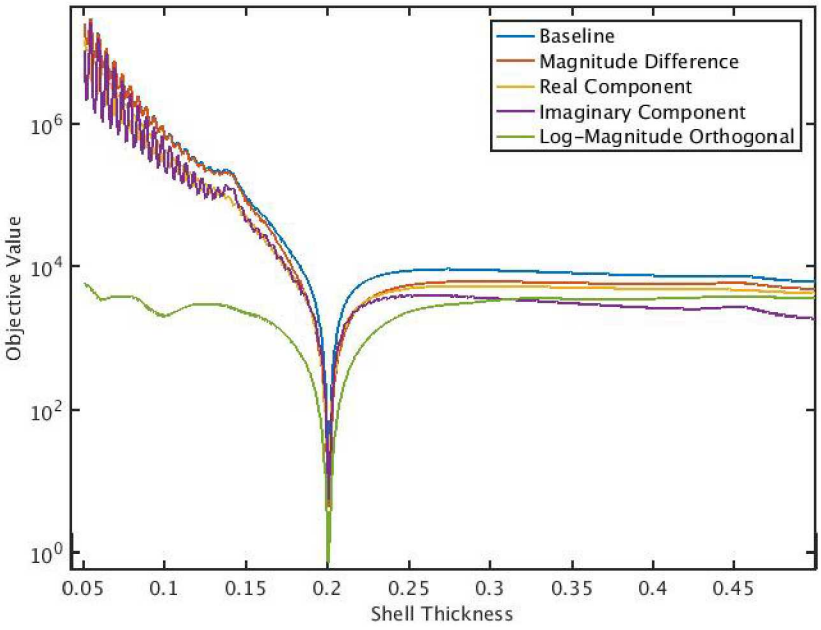

Figure 4.7: Comparison of FRF Match Error Measures on Log scale.

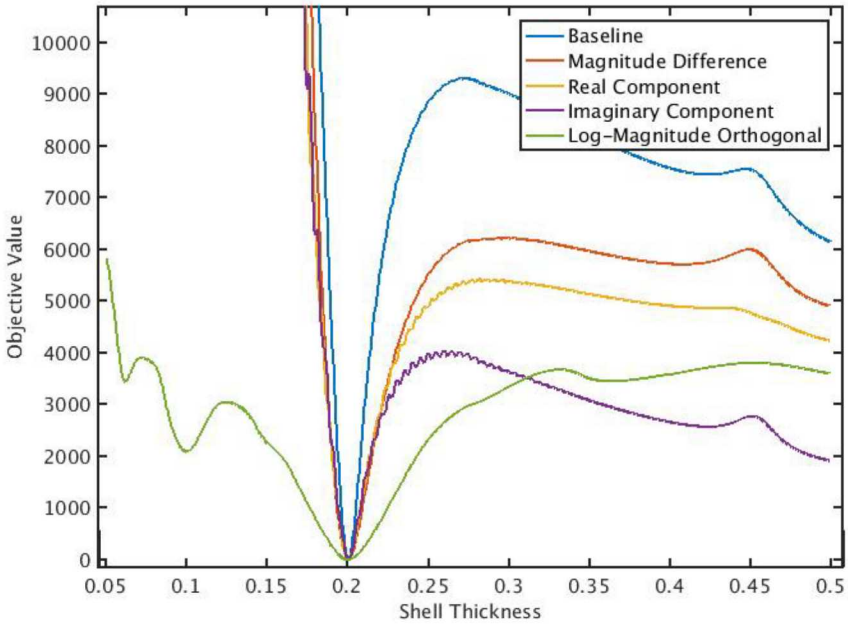

Figure 4.8: Comparison of FRF Match Error Measures on Log scale.

Test Bed Fixture Optimization Setup

As stated in the Introduction, the purpose of this research was to satisfy a Level 2 Milestone. For convenience, the completion criteria is repeated here and is as follows: A test fixture providing improved replication of mechanical environments will be designed using PLATO topology optimization for a test bed component. Using SIERRA finite element analysis, evaluate the component using (1) the test bed assembly, (2) a rigid fixture, and (3) the optimally made test fixture. The optimally made fixture will provide an improvement over the rigid fixture when compared to the test bed assembly.

The first task toward completing the Level 2 Milestone was to develop a test bed assembly. Figure 4.9 is the proposed test bed assembly with the red and yellow blocks being the component or unit under test and the green block being the next level of assembly. The assembly in Figure 4.9 was the field configuration. The field configuration was in a free-free condition with no displacement boundary conditions, i.e. free-free.

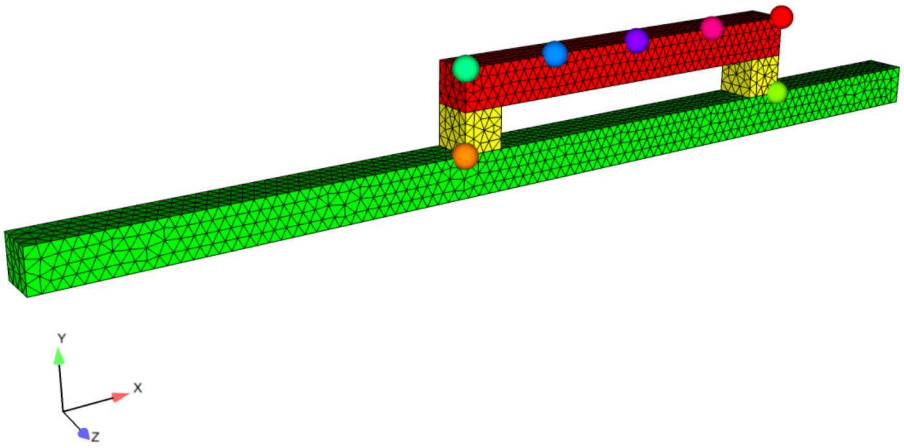

Figure 4.9: Test bed hardware and nodes used for the FRF matching optimization analysis.

For the purpose of this milestone, the typical method of testing with a "rigid" test fixture was compared to testing with an optimized test fixture. A picture of the test bed assembly with a rigid fixture can be seen in Figure 4.10. The rigid fixture was modeled by using the next level of assembly and tying all of its degrees of freedom on its bottom face to a concentrated mass with rigid bar elements. This forced all of the degrees of freedom on that face to move with zero relative displacement, acting as a rigid fixture.

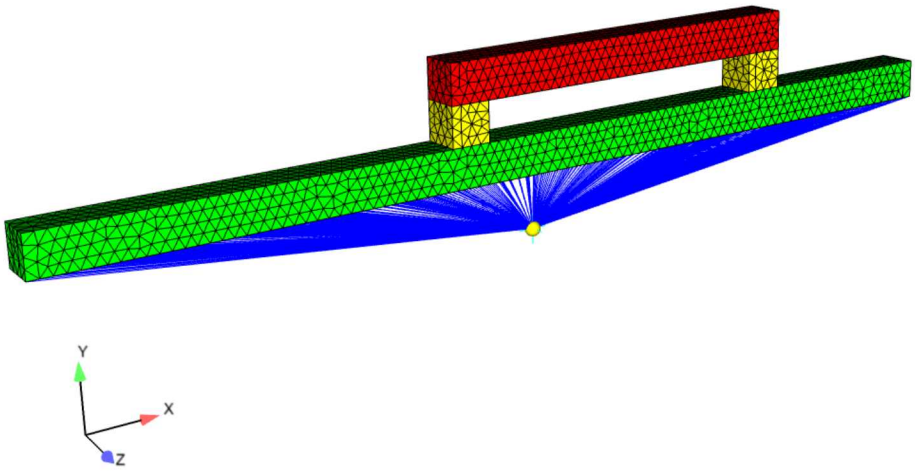

Figure 4.10: Test bed hardware mounted to a "rigid" fixture. The fixture was rigidized by tying the next level of assembly to a concentrated mass via rigid bar elements.

Current methodology was used to develop the laboratory input environment. This methodology measured an acceleration response at the base of the component of interest in the field environment. The measured response was then enforced on the rigid test fixture in the laboratory configuration so that the base of the component would have the same acceleration profile as the field configuration. This method and process is illustrated in Figure 4.11.

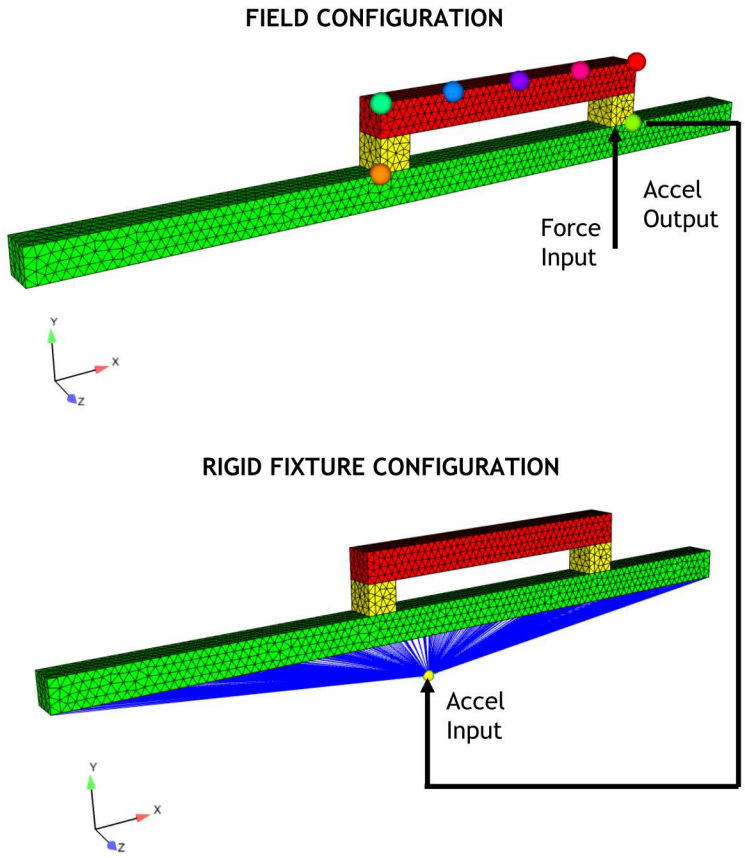

Figure 4.11: Illustration of how a typical structural dynamics test derives its input for a laboratory test with a rigid fixture.

To create a topology optimized test fixture that would replace the rigid fixture and the method of testing using the rigid fixture detailed above, an initial model was created for the topology optimization analysis. This initial optimization model can be seen in Figure 4.12. The initial model connects the component to a section of the next level of assembly shown in the green section in Figure 4.12. At the edges of the green section were two large bricks which were used as the design space for the topology optimization. A section of the next level of assembly was used because it is common for the test engineer to have prior knowledge of the next level of assembly. It is also worth noting that the field configuration does not fit into the initial optimization model, so the trivial solution does not exist.

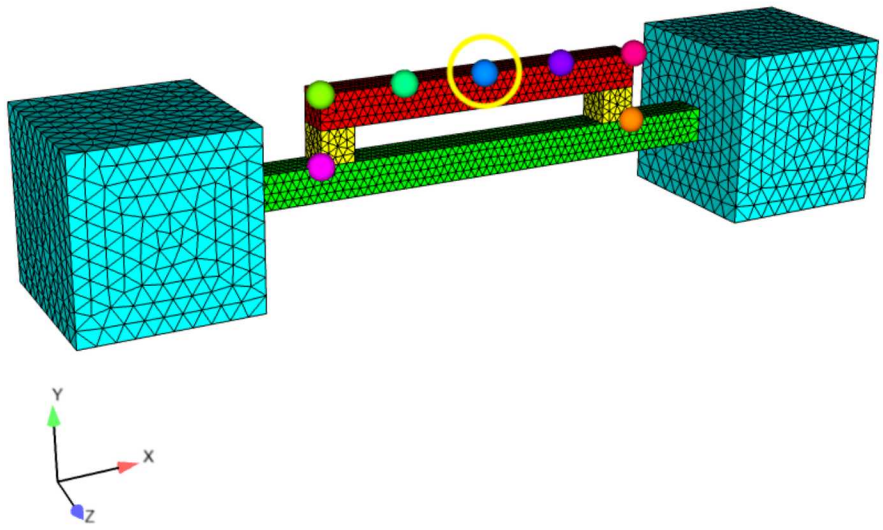

Figure 4.12: Initial model for the topology optimization model. The cyan blocks were the design space.

Exploration of Optimization Parameters

Initial Geometry Dependence

It is well known that the initial geometry impacts the optimization result for levelset methods. This was studied with a simple example of either initially a) completely filling the design domains with material b) only filling a volume in that is of similar size to the next level assembly beam. The filled barbell geometry is shown in Figure 4.13, the smaller initial geometry is shown in Figure 4.14. The FRF for the circled node in Figure 4.12 in the Y-direction was the measurement point for the initial geometries is shown in Figure 4.15. After 235 optimization iterations, which results in a stagnated geometry, the FRFs of the resulting geometries are as shown in Figure 4.16. The filled design, which began with a close match of FRF peaks has clearly done a relatively better job of matching the reference peaks. The smaller initial design has stagnated after aligning only the 590 Hz peak in the reference data. The final geometries for these results are shown in Figures 4.17 and 4.18, which are also clearly quite different.

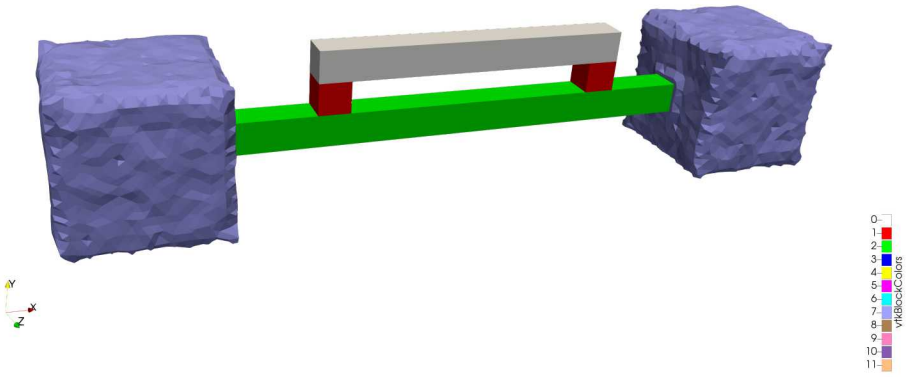

Figure 4.13: Baseline Initial Design for Optimization Parameter Comparisons.

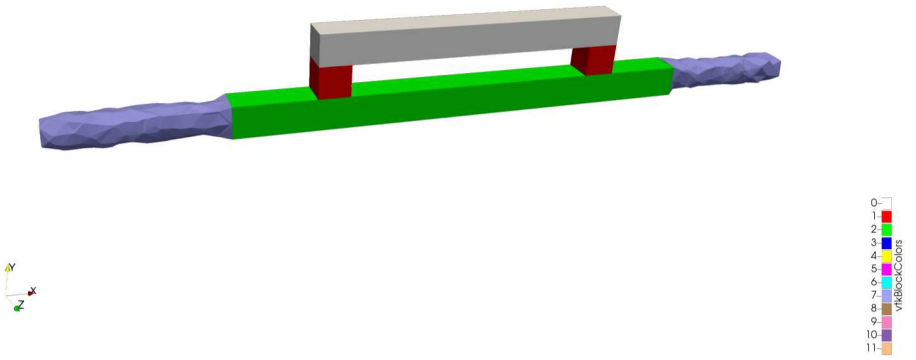

Figure 4.14: Small Initial Design for Optimization Parameter Comparisons.

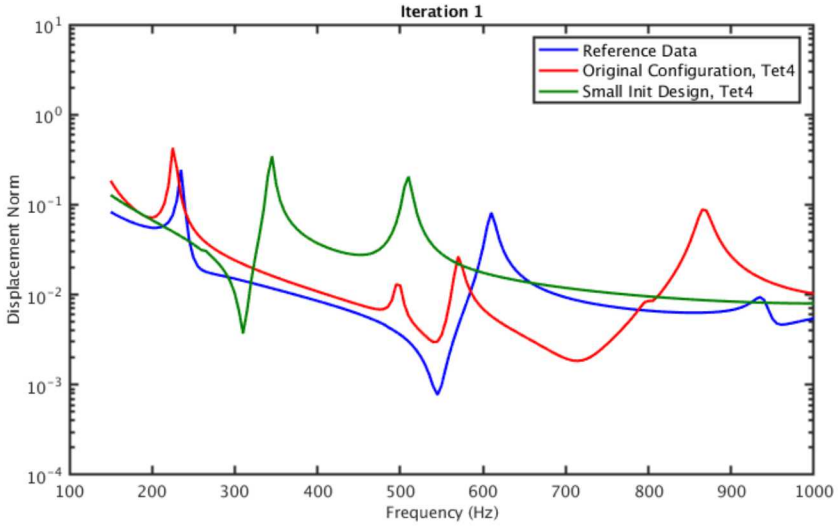

Figure 4.15: FRF comparison for beam midpoint with initial geometries.

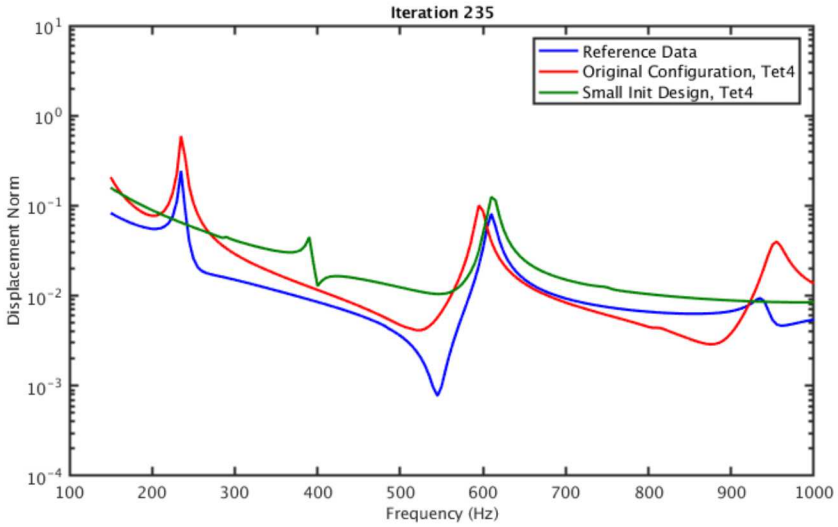

Figure 4.16: FRF comparison for different initial geometries.

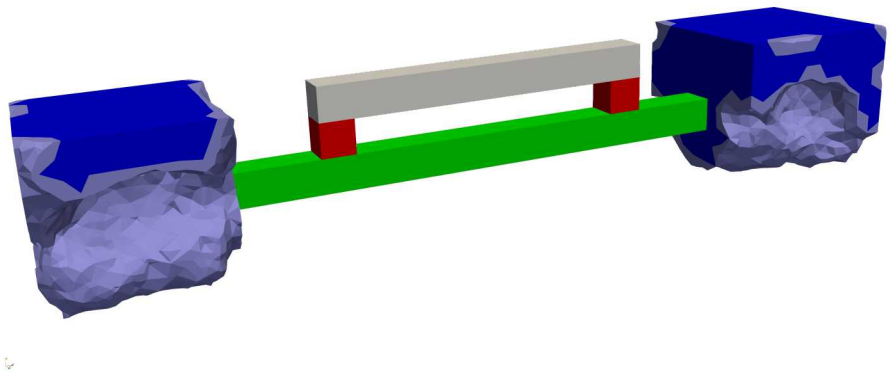

Figure 4.17: Final design geometry for baseline configuration.

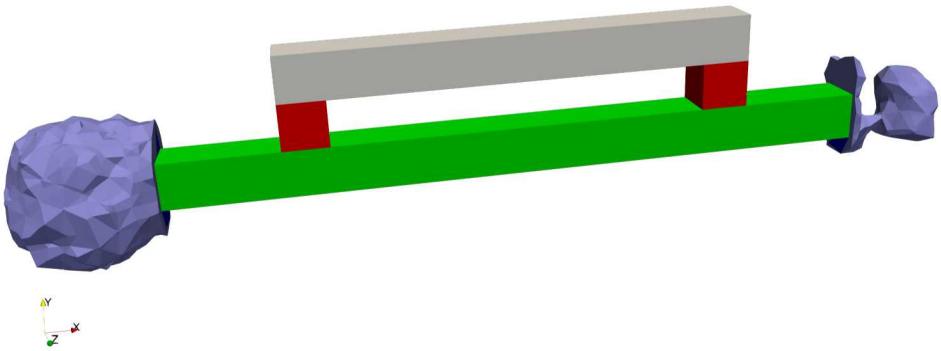

Figure 4.18: Final design geometry for configuration with small, beam-like initial geometry.

FRF Match Measure Influence

We show here the impact of changing between the two most interesting FRF match measures: that of Equation 3.15, the baseline, complex FRF measure (used elsewhere in this work); and that of Equation 3.20, the orthogonal distance measure. The resulting FRFs are shown in Figure 4.19, similar in many ways, neither being obviously a much better fit. The geometry resulting from the use of the orthogonal distance measure is shown in Figure 4.20. The initial design for this and all subsequent comparisons will be the fully filled design domain.

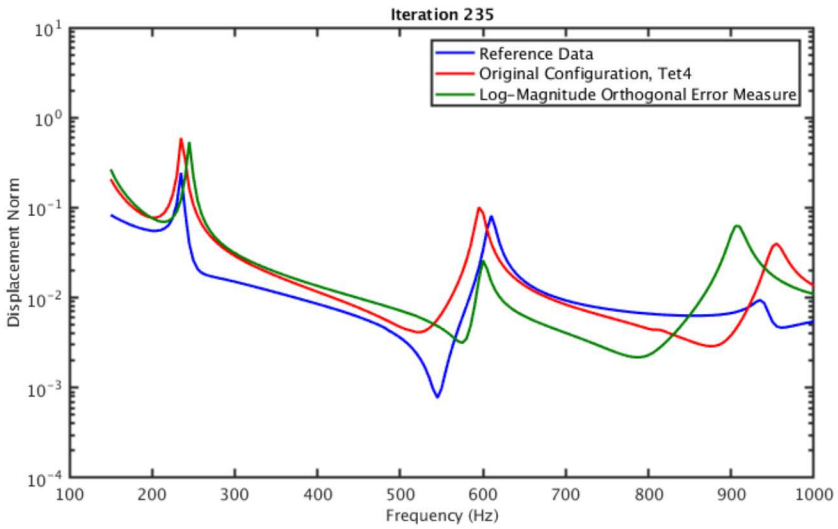

Figure 4.19: FRF comparison for varying error measures.

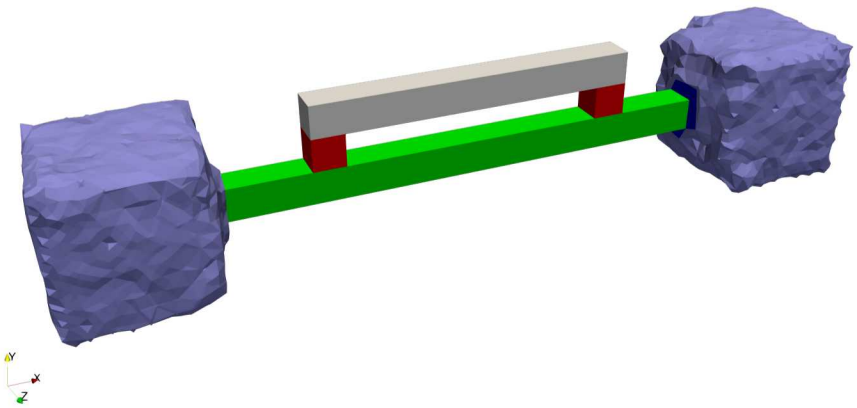

Figure 4.20: Final design geometry for orthogonal distance FRF match measure, Equation 3.20.

Optimization Algorithm Dependence

Two optimization algorithms were readily available for this problem: Kelly-Sachs Bound Constraint (KSBC) and the Global Method of Moving Asymptotes. KSBC was used for all other results shown in this report. The comparison of resulting FRFs is shown in Figure 4.21. The responses are very similar, the resulting geometry from GCMMA, Figure 4.22, is notably different than that of KSBC, Figure 4.17. This demonstrates, as was implied in earlier comparisons, that particular FRFs for this problem may likely not have unique geometry solutions.

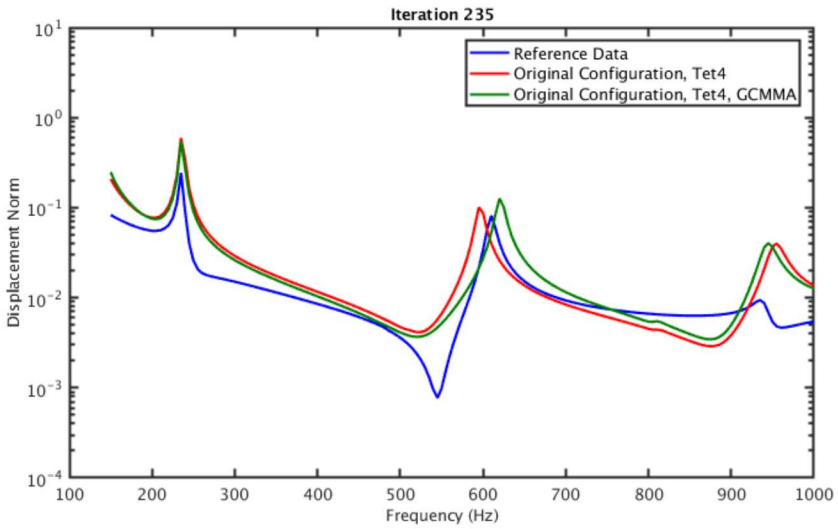

Figure 4.21: FRF comparison for different optimization algorithms, KSBC and GCMMA.

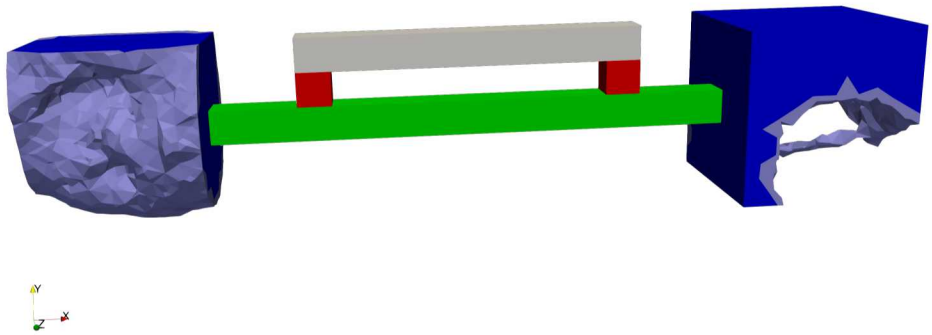

Figure 4.22: Final design geometry for GCMMA Optimization Solver.

Impact of Volume Penalty

Volume penalties or constraints are commonly used to regularize topology optimization problems. We demonstrate the effect of a volume penalty on this FRF match problem here, choosing the penalty coefficient c_v such that the initial volume penalty is 10% of the initial FRF match objective term. The resulting FRF is shown in Figure 4.23. The volume penalty has little impact on the FRF match but does have a noticeable impact on the resulting geometry, shown in Figure 4.24.

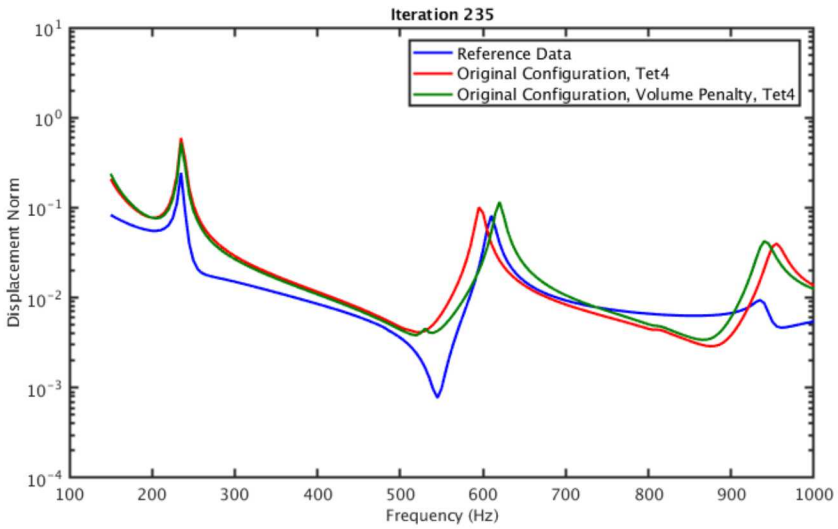

Figure 4.23: Impact of volume penalty on FRF match.

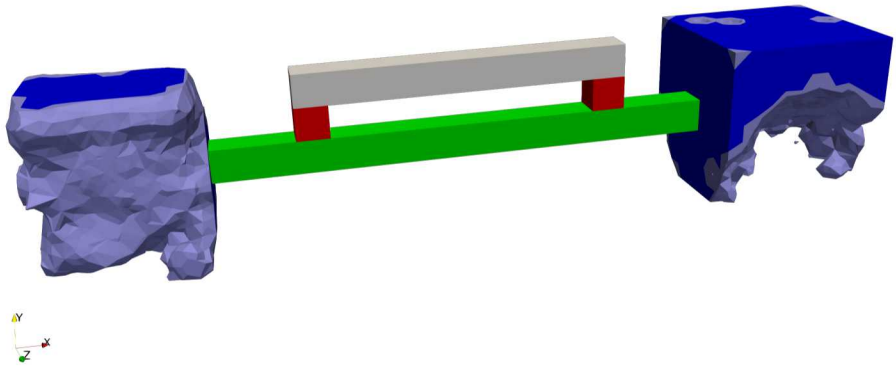

Figure 4.24: Final design geometry for configuration with volume penalty on objective.

Evaluation of Design for Milestone Criteria

The final solution used for the comparison to the rigid fixture to satisfy the completion criteria of this Level 2 Milestone was done in two steps. The first was to match the FRFs in the frequency band of 60 Hz - 160 Hz. There were no flexible modes in this frequency range. Solving this frequency range optimized the model to match the mass properties of the field configuration. The FRFs chosen for the objective function were the X, Y, and Z degrees of freedom of the nodes highlighted in Figure 4.9 and 4.12 and the input shown in field configuration in Figure 4.11. The difference between FRFs in the field configuration and

the optimized configuration per frequency line was the definition of this objective function and method of calculating the error.

The result of the optimization in the frequency band between 60 Hz and 160 Hz was used as the initial configuration for a sequential optimization run that optimized on the same objective function as before except it optimized over the 60 Hz to 300 Hz range. This range included the first elastic mode of the field configuration. The optimization iterated twelve times. The error was normalized to the error in the first iteration and the plots of the FRFs for the specified iteration can be seen for six of the iterations in Figures 4.25 and 4.26. The FRF plots in Figures 4.25 and 4.26 were of the magnitude of the displacement of the node in the center of the component.

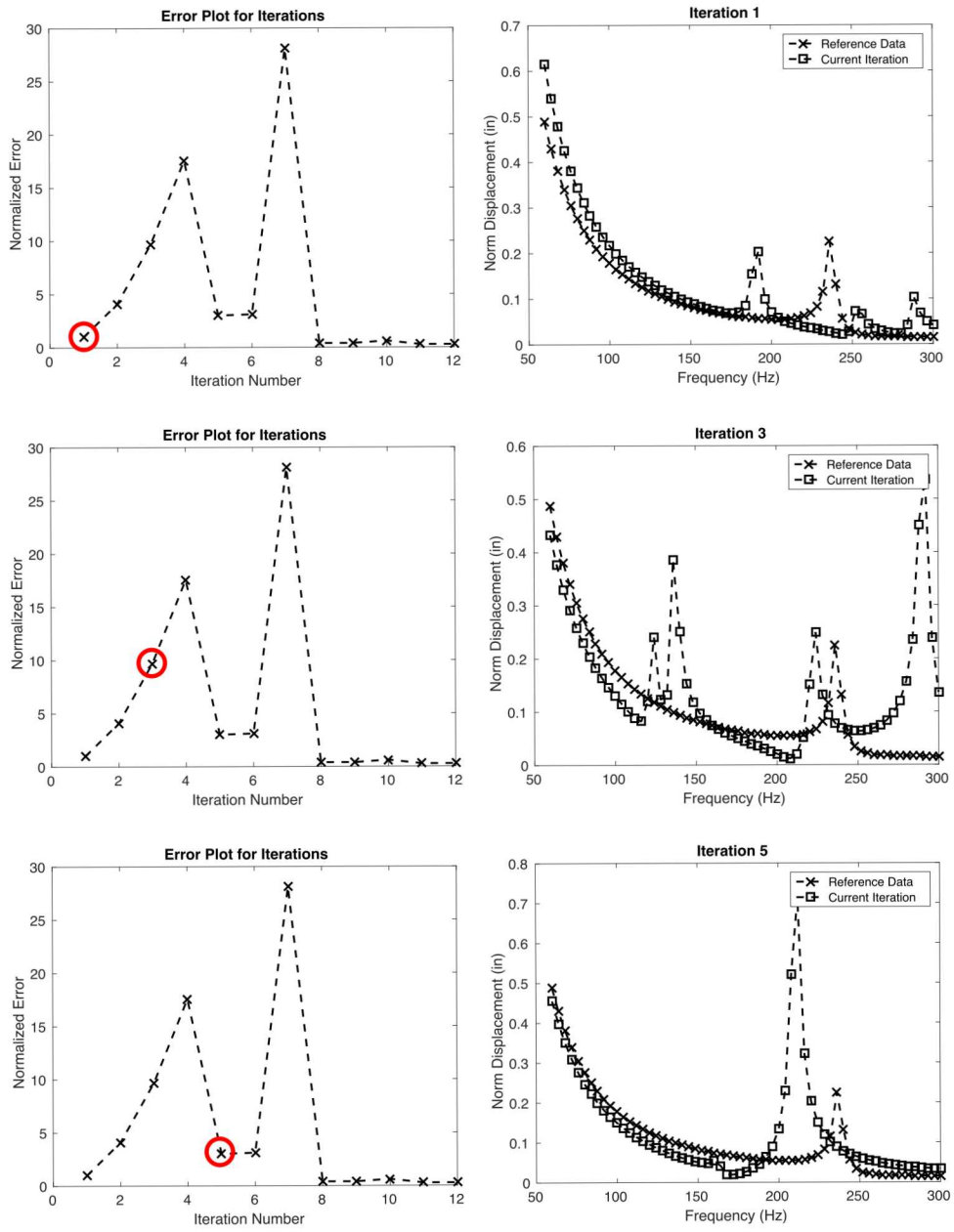

Figure 4.25: Error and FRF plots for iterations 1, 3, and 5 of optimizing over the 60 Hz to 300 Hz range.

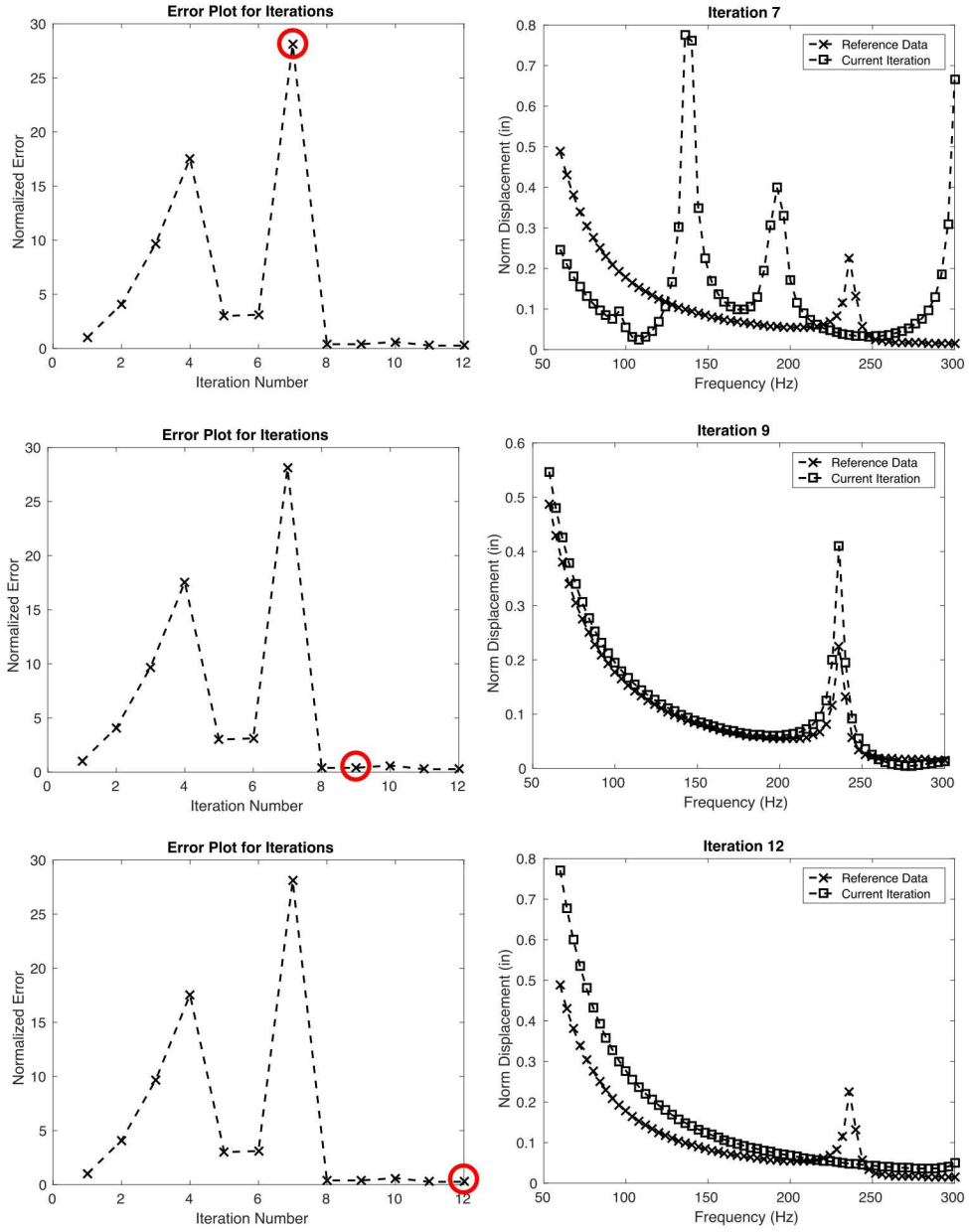

Figure 4.26: Error and FRF plots for iterations 7, 9, and 12 of optimizing over the 60 Hz to 300 Hz range.

Upon examination of the error and FRF plots in Figures 4.25 and 4.26, there were several aspects of the optimization that deserved to be noted.

- Iteration 1 showed generally good agreement in the lower frequencies. This was due to the first optimization that was run between 60 Hz and 160 Hz.
- The error plot did not show smooth convergence to a minima. Instead, the error increased and decreased multiple times into different areas of different local minima.

This was due to the aggressive parameters chosen for the optimization algorithm. The points chosen per iteration were few and they reached far from the initial location and sometimes increased in error.

- The FRFs did not have a smooth transition from one iteration to the next. Modes were introduced or eliminated depending on the iteration.
- The 9^{th} iteration had a natural frequency at the correct frequency, however, the optimization stiffened that natural frequency to lower the error in iteration 12. The error for iteration 9 was 0.39 and 0.26 for iteration 12.

When selecting which iteration would provide the best test fixture, the result from iteration 9 was selected over iteration 12 because iteration 12 had no natural frequency in the frequency of interest. This meant that the fixture was rigid in the frequency of interest and would be the same as the rigid fixture which would provide no benefit. The finite element model of the optimized fixture for iteration 9 is shown in Figure 4.27 with the compared point in the FRF figures identified.

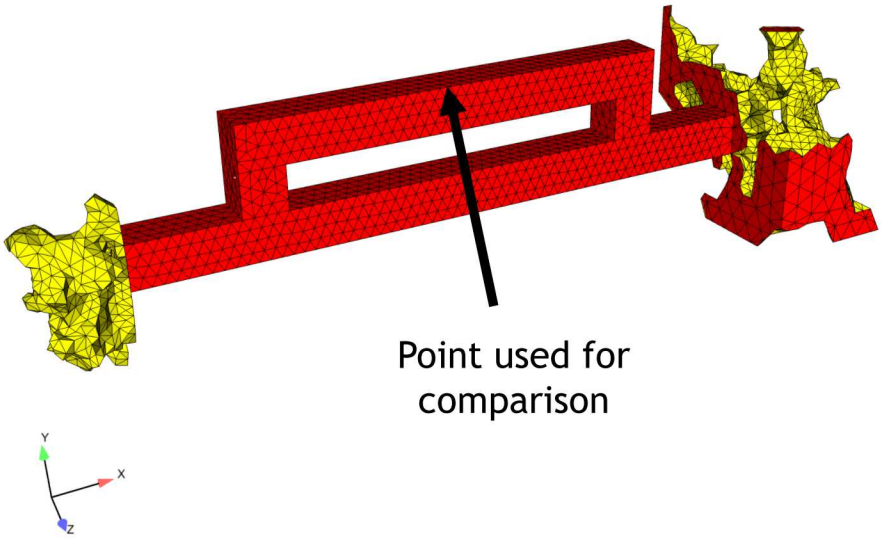

Figure 4.27: Topology optimized test fixture derived from iteration 9 optimized over the frequency range 60 Hz to 300 Hz.

The note above that addressed the fact that iteration 12 had lower error than iteration 9 deserves additional investigation. In iteration 9, the lower frequencies matched and the natural frequency was correct. The only deviation between the two FRFs was the amplitude of the FRFs at the natural frequency. From the Theory section in Chapter 2, the amplitude of the frequency response function at the natural frequency is the mode shape. Figures 4.25 and 4.26 only show the FRFs from one degree of freedom. If the amplitude at the natural

frequency isn't scaled the same over all degrees of freedom, then the shape is different along with the stress field for that shape. This raised the error calculated and no resonance was calculated to be a lower error.

To determine the differences in the shapes, a modal analysis was computed on the field configuration and the optimized model. Snapshots of the mode shapes at approximately 230 Hz are illustrated in Figure 4.28. At first glance, it appears that the two shapes were very different as the majority of the motion in the field configuration is in the Y direction and the majority of the motion in the optimization configuration was in the Z direction. After closer examination, the nodes of each mode had similar locations and there was some deflection in the Y direction in the optimization configuration's mode.

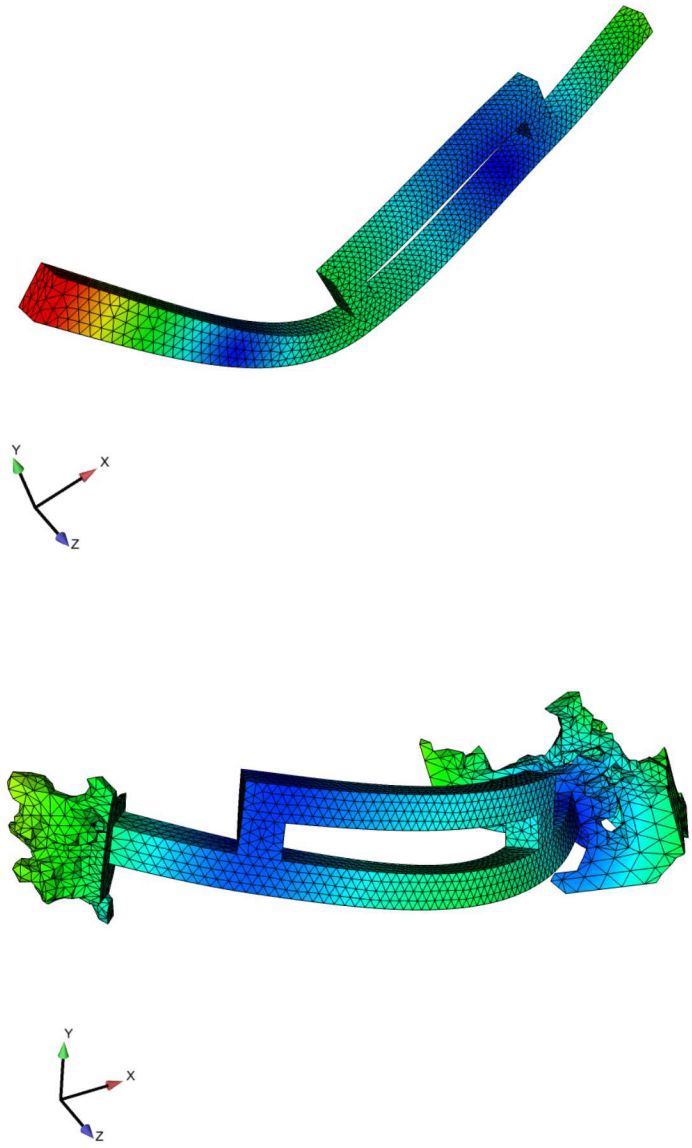

Figure 4.28: First elastic mode shape of the field configuration (top) and the optimization configuration (bottom).

To determine if the optimized test fixture was an improvement over the rigid fixture, both were tested analytically in a simulated laboratory test. The method of how the environment was calculated and how the laboratory test was designed for the rigid fixture was previously described and illustrated in Figure 4.11.

The force input for the optimization configuration was placed at the same location as it was for the optimization problem shown in Figure 4.29. To derive the laboratory test's forcing function, the frequency response functions between the degrees of freedom used in

the optimization problem in Figure 4.12 and the forcing function was used. These FRFs were inverted using its pseudo-inverse to calculate the best forcing function to excite those response degrees of freedom in the same way that they were excited in the field environment.

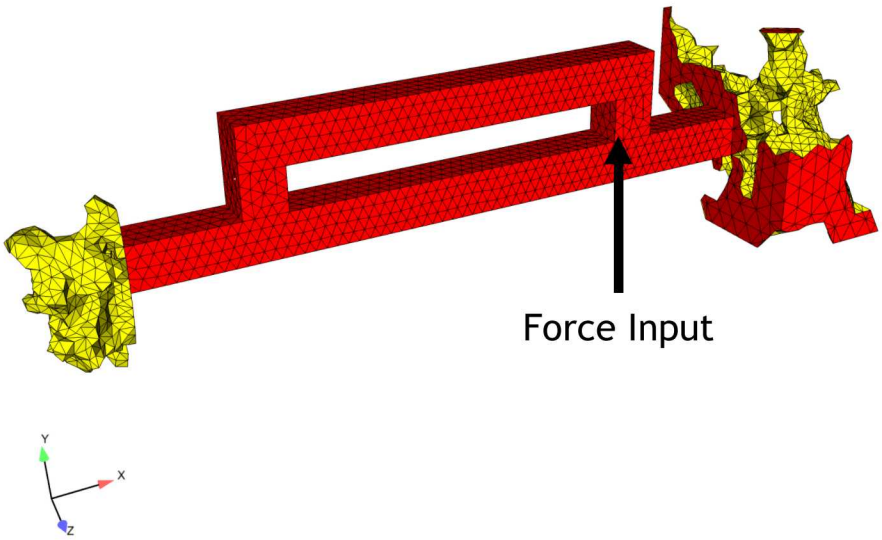

Figure 4.29: Laboratory setup for the optimization configuration.

With both simulated laboratory tests defined, the stresses from them were calculated. The Von Mises stress was calculated per frequency line and the total stress was calculated as a root mean squared (RMS) value per

$$x_{rms} = \frac{1}{n}\sqrt{\sum_{m=1}^{n} x_m^2} \tag{4.1}$$

where x is the variable of interest, and n is the total number of discrete points in the signal. The plots of the Von Mises stresses for the field, optimzation fixture laboratory, and rigid fixture laboratory configurations can be found in Figure 4.30, 4.31, and 4.32 respectively. Several comparisons can be drawn from these results.

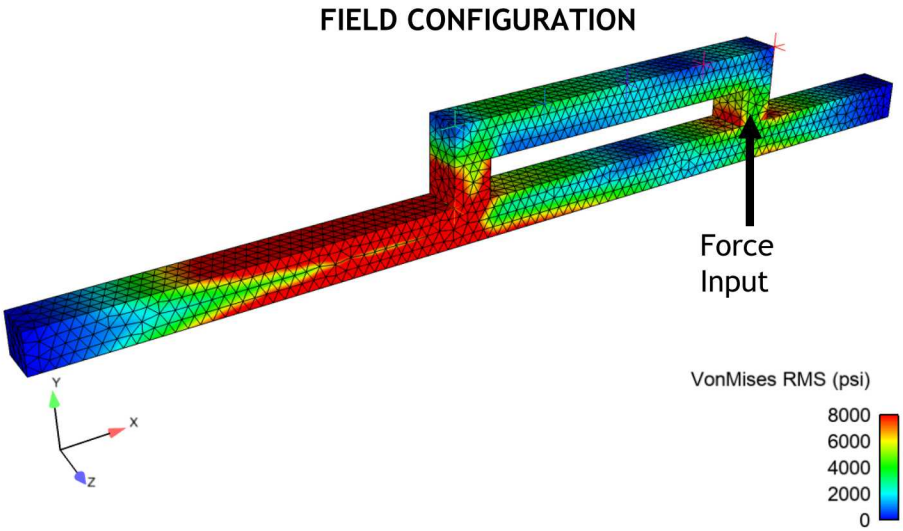

Figure 4.30: RMS response of Von Mises stress for the field configuration and environment.

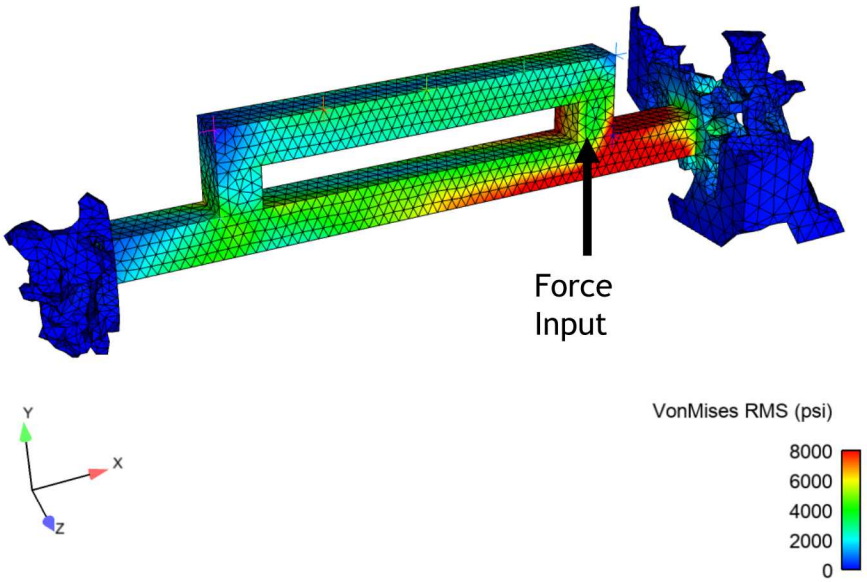

Figure 4.31: RMS response of Von Mises stress for the optimization configuration and laboratory environment.

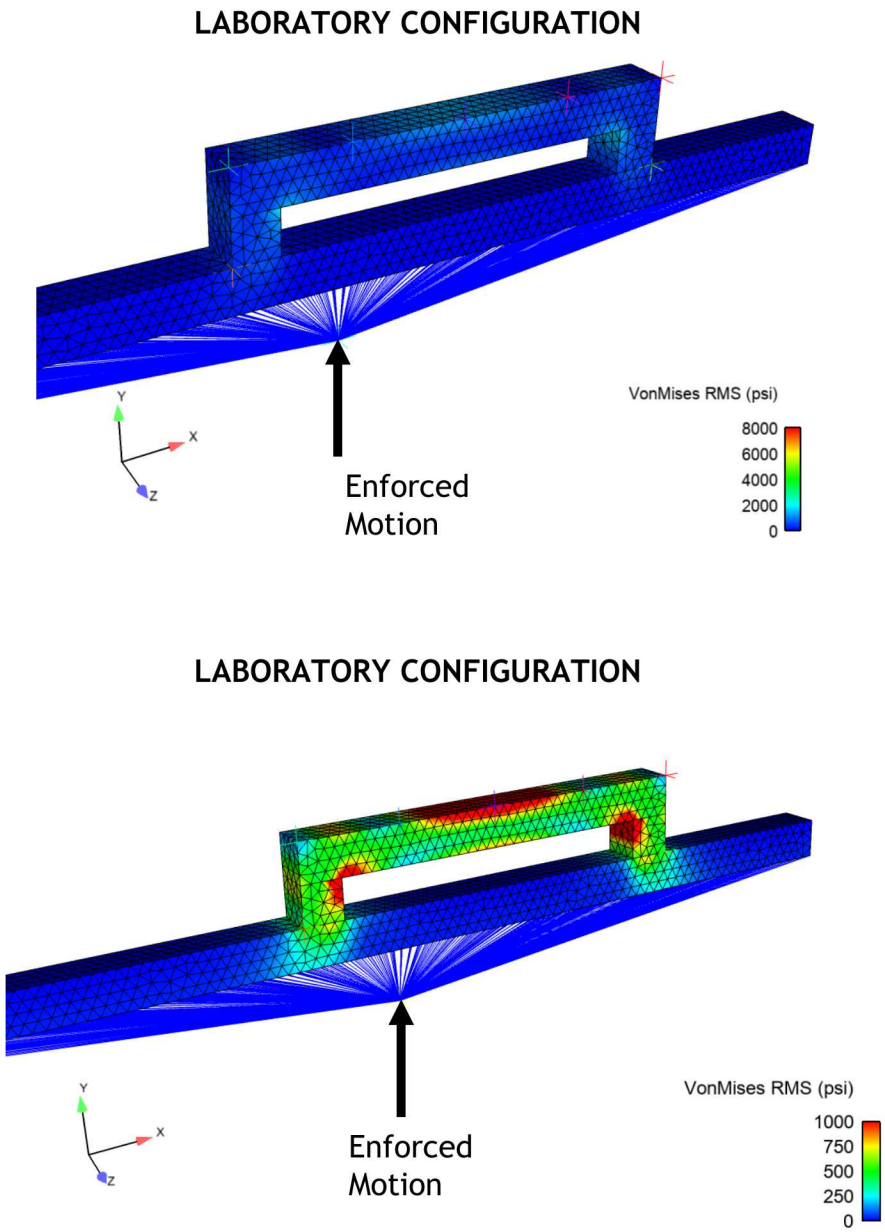

Figure 4.32: RMS response of Von Mises stress for the rigid configuration and laboratory environment. Common colormap to other configurations (top) and rescaled colormap (bottom).

To quantifiably state the differences between the field environment and the two different laboratory environments, the Von Mises stress was compared at 5 discrete locations and the error was calculated. The five locations that were chosen for comparison are shown in Figure 4.33. The quantified difference between the environments can be found in Table 4.2.

Table 4.2: Approximate RMS Von Mises stress of the Field Configuration, Rigid Configuration and Optimized Configuration and their associated errors

Node #	VM Stress Field	VM Stress Rigid	VM Stress Optimization	Rigid Error	Optimization Error
1	8 ksi	0.5 ksi	4 ksi	94%	50%
2	8 ksi	1 ksi	3 ksi	88%	63%
3	2 ksi	1 ksi	4 ksi	88%	50%
4	5 ksi	1 ksi	5 ksi	88%	38%
5	8 ksi	0.5 ksi	8 ksi	94%	0%

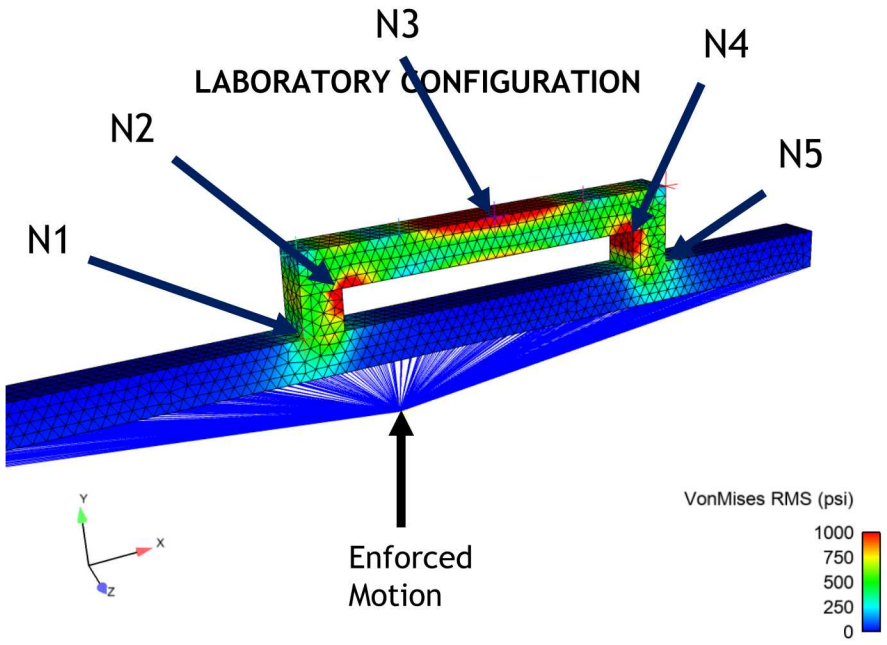

Figure 4.33: Location of nodes used for stress comparisons between the different hardware configurations.

Figures 4.30 through 4.32 and Table 4.2 show that even though the optimization laboratory configuration was not a perfect match to the stress in the field configuration, it was an improvement over the rigid laboratory configuration. Through qualitative examination of the general stress field in Figures 4.30 through 4.32, the stress from the first elastic mode shape was proportional to the result because only one mode for each configuration is excited. With the rigid fixture, all of the motion concentrates to the 90 degree bends in the component and the top part of the beam. In contrast, with the connection degrees of freedom allowed to move like the field configuration, the optimized test fixture provided a more realistic

boundary condition which spread out the stress on the component. Also, Figure 4.28 shows the qualitative difference between the optimized fixture configuration's mode shape and the field configuration's mode shape. The field configuration's mode shape had significant motion in the Z direction which placed a even strain on the top member of the component that isn't experienced by the field configuration. This result is seen when comparing Figure 4.30 and 4.31.

One could argue that if this information was known a priori to the laboratory test, the input specification for the rigid fixture configuration could be amplified by a factor of approximately 16 in order to make sure that the stress in the laboratory was at least as much as it was in the field. However, due to the boundary conditions and the stress field of the rigid laboratory configuration, the stress at the middle of the component would be an over test by approximately a factor of 8 and could cause a failure that would not be experienced in the field.

Chapter 2 stated that the responses, displacement and stress, are a result of a convolution between the input forcing function and the dynamic frequency response functions of the system which consists of the component and its next level of assembly or its test fixture. Although the comparison between the optimized fixture and rigid fixture in Figures 4.31 and 4.32 reflect what test can be run on the optimized fixture and what is run on the rigid fixture today, the methods for applying the forcing function in method and location were different and, therefore, influenced the comparison between the rigid fixture and optimized fixture.

In an effort to remove the effect of the forcing function's effect on the comparison between the rigid fixture and the optimized fixture, the method of deriving an input force that was used on the optimized fixture was applied to the rigid fixture. Two changes were made to the original laboratory configuration in order to modify it to match the laboratory configuration of the optimized fixture. First, the rigid elements connecting the next level of assembly to a concentrated mass and the concentrated mass were removed. Next, the modulus of the next level of assembly beam was increased by a factor of 100. These steps created a "rigid" fixture that had free boundary conditions which matched the configuration of the optimized laboratory configuration.

With the new laboratory configuration, the process of applying a force that was derived by multiplying the inversion of the rigid fixture assembly's frequency response functions with the responses from the field environment was performed. This forcing function was applied at the same location as was referenced in Figure 4.29 and was derived using exactly the same method as was done to the optimized test fixture. The two forcing functions were compared and can be seen in Figure 4.34.

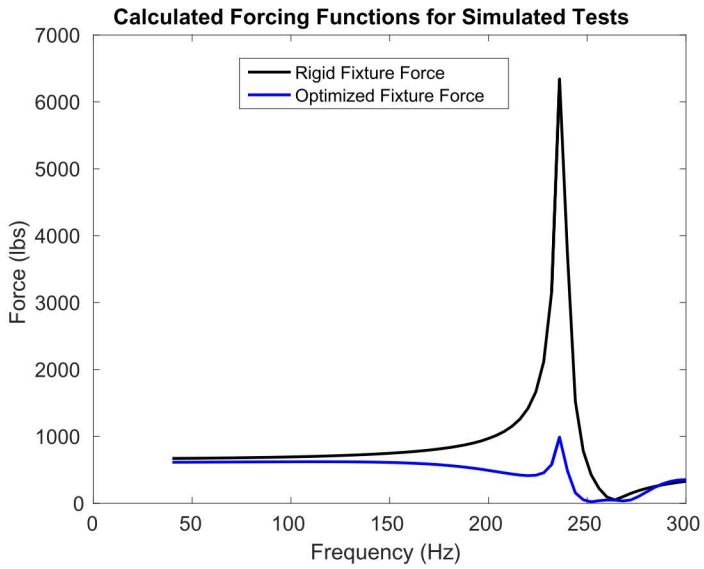

Figure 4.34: Calculated input forces for the optimized laboratory configuration and the free rigid laboratory configuration.

Figure 4.34 shows that the forcing function calculated for the rigid fixture was approximately a factor of 6 higher than the forcing function for the optimization forcing function. The reason for this difference in force magnitude lies in the aforementioned force inversion process. The force inversion process calculates a forcing function that gives a least squared error fit to the response data it is given. Because the mode shape of the rigid fixture configuration differs from the field configuration more than the optimized configuration, the derived forcing function was larger in an attempt to compensate for the inappropriate boundary conditions.

Stresses were calculated using the forcing function for the rigid fixture shown in Figure 4.34 into its respective laboratory configurations. The resultant stresses are shown in Figure 4.35. They qualitatively show similar results to the rigid fixture with the enforced motion input. This indisputably shows that the forcing function cannot change the response field. This is due to the fact that the only elastic mode shape being excited in this frequency range is not modified by the forcing function, but rather the mode shape is only modified by the test fixture to which it is attached.

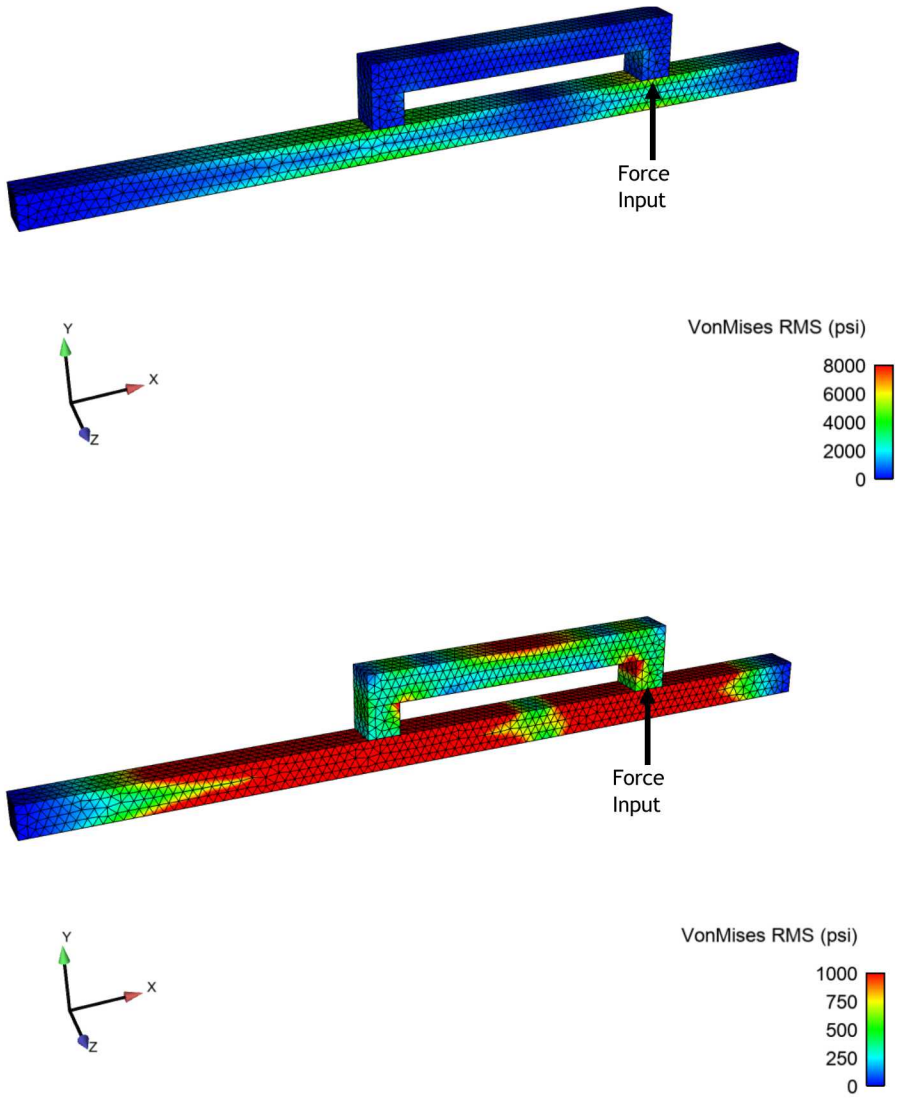

Figure 4.35: Resultant stresses of the laboratory environment with a rigid fixture and a calculated input force. Top figure's stress is scaled identically to the optimized laboratory configuration and field configuration. Bottom figure's stress is scaled for qualitative evaluation.

Chapter 5

Quantifying and Calculating the Error Caused by the Test Fixture

During the course of this research, what constituted a good test fixture was unknown. This was due to there being no known quantity that defines a metric that ties the test fixture to the success of a laboratory test. This section explores that question and defines a metric that provides some insight into the fixture's ability to make a laboratory test successful.

To develop a metric to quantify the test fixture's ability to replicate the field environment, a successful laboratory test needs to be defined. The majority of structural dynamic testing that is executed in the laboratory has the purpose of determining if the component will mechanically fail when it is in its intended field environment. This goal of replicating the correct stresses in the correct locations to reproduce failure modes in the laboratory environment is the basis of the success of the test. Although the test fixture design plays a critical role in the responses, the responses of the component are the convolution between the input forcing function and the system's transfer functions or frequency response matrix shown as

$$\mathbf{H} \cdot \bar{F} = \bar{x}, \tag{5.1}$$

where $\bar{F}$ is the column vector of external forcing function vector acting on the degrees of freedom of the system, $\mathbf{H}$ is the system's frequency response matrix and $\bar{x}$ is the column vector of responses of the system. The frequency response matrix is symmetric and is a function of the mass, stiffness, and damping of the structure. If the frequency response functions are examined in the modal domain, they are functions of the mode shapes, natural frequencies, and modal damping.

Due to the responses of the component being a function of the external forces and the configuration's frequency response matrix, it is inherently difficult to determine what responses are possible to achieve from a given configuration or frequency response matrix. The following theory examines the lab configuration in comparison to the field configuration in the modal domain. The theory follows that if the mode shapes of the laboratory configuration span the same space as the mode shapes excited in the field environment, then there exists a forcing function that can excite the laboratory configuration to have the same responses

as the field configuration.

To quantify the test fixture's ability to replicate the dynamics of the next level of assembly in the field configuration, a successful laboratory test is defined as

$$\bar{x}_F = \bar{x}_L \tag{5.2}$$

where $\bar{x}$ is a vector of response displacements, the subscript F designates the field environment and the subscript L designates the laboratory environment. This criteria is acceptable to determine a successful test because if the displacements between the two systems are matched, the stress states at that given moment in time are matched given identical systems. Linear modal analysis theory states that the displacements of a system can be defined by a linear combination of all of the system's mode shapes. Practically this substitution is written as

$$\bar{x} = \sum_{m=1}^{\infty} \boldsymbol{\phi_m} q_m \tag{5.3}$$

where $\boldsymbol{\phi_m}$ is the m^{th} mode shape of the system and q_m is the m^{th} modal coefficient that correspond to its respective mode shape. The displacements in Equation 5.3 can be represented in the time or frequency domain and the designation is dropped for brevity.

Including an infinite amount of modes is impractical in most engineering applications, therefore, a finite number of modes are made to approximate the physical displacement:

$$\bar{x} \approx \sum_{m=1}^{n} \boldsymbol{\phi_m} q_m. \tag{5.4}$$

Only the modes up to the n^{th} mode are included in Equation 5.4. Since not all of the modes are included in the modal substitution, the expression in Equation 5.4 is an approximation and the error in the displacement is referred to as modal truncation error. The modal substitution from Equation 5.4 is rewritten in matrix form and is substituted into Equation 5.2

$$\boldsymbol{\phi}_L \bar{q}_L = \boldsymbol{\phi}_F \bar{q}_F. \tag{5.5}$$

To determine the modal coefficients of the laboratory mode shapes, the pseudo-inverse of the laboratory configuration's mode shapes are pre-multiplied to both sides

$$\bar{q}_L = \boldsymbol{\phi}_L^{+} \boldsymbol{\phi}_F \bar{q}_F \tag{5.6}$$

where the $^+$ symbol designates a Moore-Penrose pseudo inverse. At first glance, it appears that Equation 5.6 calculates the $\bar{q}_L$ values that need to be excited to match the responses of the laboratory configuration to the responses of the field configuration. However, the multiplication of the pseudo inverse is only a projection of the field configuration's mode shapes to the laboratory configuration's mode shapes. Because the mode shape matrix introduced in Equation 5.4 is truncated, the mode shape matrix is rectangular and the error of the projection is minimized in a least squared sense.

To determine the error created by this projection, one can compute the physical displacements by using the given modal coordinate, q_F, and calculated modal coordinate, q_L, with their respective mode shapes to get Equation 5.2 and then compute the difference between those vectors. Although this would give you the error in the physical domain, it would be of interest to know the error of the projection in the modal domain to determine the source of the error and determine the error's impact with respect to the mechanical environment.

To calculate the error in the modal domain, the error per field mode is examined. Equation 5.6 is rewritten as

$$\bar{q}_{Ln} = \boldsymbol{\phi}_L^+ \bar{\phi}_{Fn}. \tag{5.7}$$

Equation 5.7 calculates what modal coordinates in the laboratory configuration are needed to minimize the error of replicating the n^{th} mode of the field configuration. The $\bar{\phi_{Fn}}$ variable is a column vector of a single mode from the set of modes from the field configuration's mode shapes for which the error is calculated. This would be equivalent to assigning the $\bar{q}_F$ vector to be zeros with a one in the index corresponding to the mode shape of interest.

With a calculated vector of modal coordinates from the laboratory configuration, the expression

$$\bar{\phi}_{Fn}^+ \boldsymbol{\phi}_L \bar{q}_L = \bar{q}_{FnReconstructed} \tag{5.8}$$

calculates the equivalent modal coordinate in the space of the single mode shape. Equation 5.8 is a projection from the laboratory mode shape space to the space of the field mode shape under inquiry. The error in the modal domain can then be computed by

$$\bar{\phi}_F^+ \boldsymbol{\phi}_L \boldsymbol{\phi}_L^+ \bar{\phi}_F = \epsilon^2. \tag{5.9}$$

The error in Equation 5.9 is squared due to the projection from the mode shape space from the field mode shape of interest to the mode shape matrix of the laboratory space

combined with the projection from the laboratory mode shape matrix space to the space of the field mode shape of interest.

Chapter 6

Alternate Objective Function for Designing a Test Fixture

The research presented in this report examines the use of using FRF matching as the objective function for designing a dynamic test fixture. Although the FRF is a valid metric for specifying the structural dynamics of a system, there are alternative representations to specify the structural dynamics of a system. This chapter covers alternate objective functions that were considered or proposed.

Chapter 2 states that stress is related to displacement which is a linear combination of the system's mode shapes. Because of this relationship, if a linear combination of mode shapes from the laboratory configuration span the space of the modes in the field configuration, then it is possible to produce the same stresses. Optimizing on matching the mode shapes between the field and laboratory configurations was presented as an option. However, calculating a stable version of the derivatives was identified as a research topic. Tracking the derivatives of the Eigen vectors of a dynamic system has difficulties and was determined to be time consuming and wouldn't fit into our timeline for this L2 milestone.

Chapter 2 introduces the framework of transforming the mode shapes of the component into the space of the component's fixed base mode shapes and it's Craig-Bampton constraint shapes. The aforementioned constraint shapes are static shapes where one boundary degree of freedom at a time is given unit displacement and the rest held fixed. It is a linear combination of these static constraint shapes that span the space of any impedance of the next level of assembly.

It is in this space that Randy Mayes first suggested that environments could be derived and specified [3]. He proposed that the fixed base modes are the main sources of stress and strain and, therefore, if they are excited to the correct levels in the laboratory test, then the test is a success. This methodology neglects to include any stress that is from the constraint shapes. From the definition above of the constraint shapes, if there is one connection from the component to the next level of assembly, then the fixed base modes are the entire sources of stress in the component.

The Craig-Bampton mode space framework can be used in the design of a dynamic test fixture using topology optimization. If the modes of the component or unit under test are transformed into Craig-Bampton shape space, it is trivial to prove that the fixed

base mode shapes between the field configuration and the laboratory configuration are automatically matched. With those shapes automatically matching, then the complete mode shape space will match if the static constraint shapes match between the field and laboratory configurations.

A static shape match objective function only needs to modify the test fixture's stiffness properties at a single frequency. This theoretically greatly reduces the number of local modes in the optimization space which plagued the FRF matching objective function. This method was discovered toward the end of the research year and was not fully explored in this body of research. In order to explore this option, the following steps would have to be executed and analyzed.

1. Perform an optimization run with the constraint shapes as the objective function
2. Calculate the mode coordinates of the laboratory configuration needed to excite the motion of the laboratory configuration to match the motion of the field environment
3. Determine the single or set of forcing functions needed to excite the modes of the laboratory configuration to match the motion of the field environment
4. Determine the feasibility of being able to impart the calculated forcing functions on an experimental set of hardware
5. If necessary, determine if optimizing on the constraint shapes solution creates a design that can be optimized using a different objective function.

Although the objective function of matching the Craig-Bampton constraint shapes was not fully explored, a single run within Optistruct was run on the BARC hardware with an objective function that was similar to matching the constraint shapes. The setup parameters for this static run is shown in Figure 6.1. Figure 6.1 shows that a single force applied at an oblique angle with respect to the axes of the structure. Although this setup is not a pure representation of the constraint shapes, it exercises a linear combination of six of the twelve constraint shapes.

The resultant fixture calculated from the topology optimization with the static objective function shown in Figure 6.2 was not subject to environment to determine how well it matched the field configuration. The error of its mode shapes calculated by the error metric from Chapter 5 was compared with the error from a rigid fixture. The error for the rigid fixture was calculated to be 0.3 and the error for the optimized fixture was 0.001 for the first elastic mode.

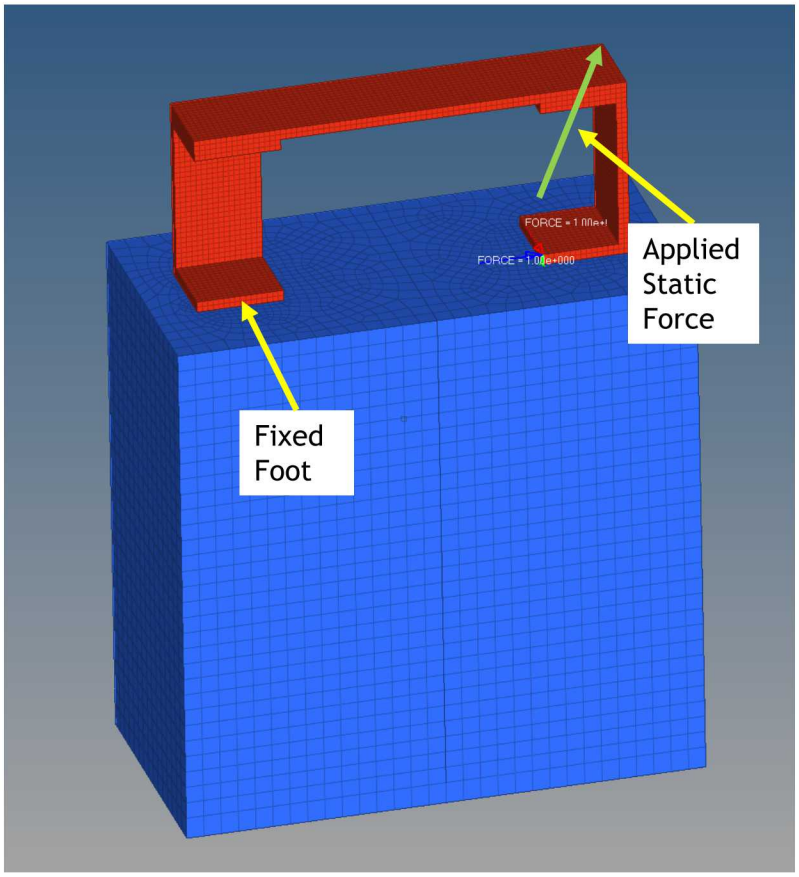

Figure 6.1: Topology optimization result of static objective function.

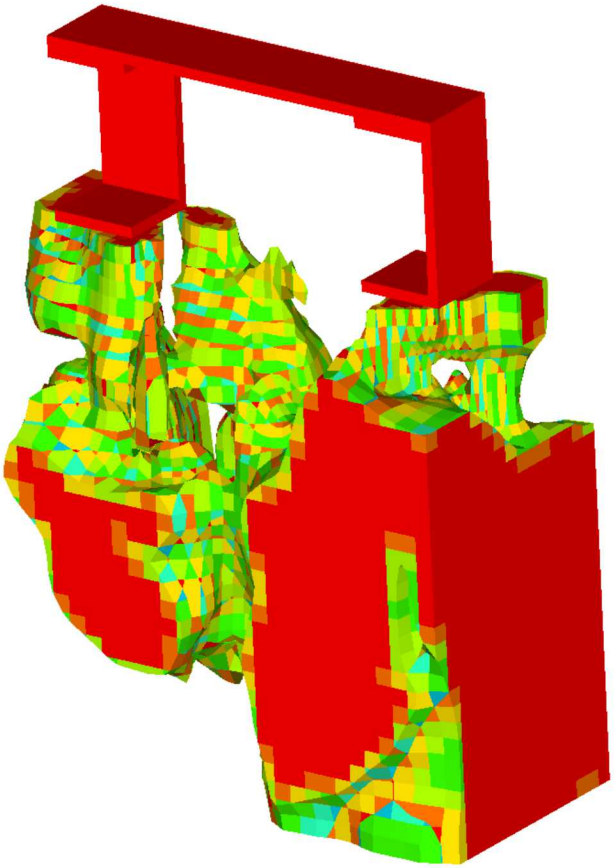

Figure 6.2: Topology optimization result using static shape matching as the objective function.

Chapter 7

Conclusions

The objective of this research was to satisfy a Level 2 milestone that addressed the design on a structural dynamic test fixture that improved the quality of a structural dynamics laboratory test. The success criteria of this milestone was that a new test fixture needed to be designed via topology optimization and the PLATO software. The optimized test fixture needed to show an improvement over a typical, rigid test fixture.

To satisfy this success criteria, the PLATO software developed the capability to optimize based on matching the frequency response functions between two structures. This objective function would satisfy the success criteria of the milestone and an ideal test fixture would be made. The PLATO software also developed levelset optimization capability, multiple element definitions, and a restart capability.

Through use of the PLATO software and an alternate topology optimization software, Optistruct, it was discovered that the optimization space is non-convex and many local minima exist in the domain. The extent and difficulty of the amount of local minima in the error domain was explored by altering several optimization parameters to determine the differences in results. These studies discovered that it is extremely difficult to converge to the global minimum.

Even though there were difficulties of optimizing based on the objective function of matching frequency response functions, a test fixture was developed for a test bed example in order to meet the success criteria for the Level 2 milestone. A test fixture was developed using the restart capability within PLATO's topology optimization algorithm using the frequency response function matching objective function.

This topology optimized test fixture was integrated into the test bed. Analytical comparisons were made between the field environment, the rigid test fixture attached to the component, and the optimized test fixture attached to the component. Through quantitative comparison to the field configuration, the optimized test fixture provided an improvement over the rigid test fixture. Though the optimized fixture was an improvement, it did not identically replicate the stress field in the field configuration because the mode shape that was excited was not the same as the field configuration. The main conclusion from these results were that using topology optimization in the same way as proposed here does not result in ideal fixtures, but it can result in an improvement over todays fixtures and processes.

In addition to completing the milestone, an error metric that quantifies the ability that the component in the laboratory can match the stress in the field was developed. This error metric was not implemented into the topology optimization process, but it provided a metric on the effectiveness of the test fixture other than comparing the responses of the field and laboratory configurations. Not only can the error metric be used for test fixture effectiveness, but it can be used in other projection analyses such as structural dynamic substructuring.

Bibliography

[1] P. Avitabile. Modal space article. *SEM Experimental Techniques*, 1999.

[2] P. M. Daborn. Smarter dynamic testing of critical structures, 2014.

[3] Randall L. Mayes. *A Modal Craig-Bampton Substructure for Experiments, Analysis, Control and Specifications*, pages 93–98. Springer International Publishing, Cham, 2015.

[4] Timothy Walsh, Wilkins Aquino, Denis Ridzal, Drew Kouri, Bart van Bloemen Waanders, and Angel Urbina. Viscoelastic material inversion using sierra/sd and rol. Technical Report SAND2014-19498, Sandia National Laboratories, 2014.

DISTRIBUTION:

1	MS 0557	John Pott, 1557
1	MS 0346	Lili Heitman, 1553
1	MS 0840	Jim Redmond, 1550
1	MS 0346	Pete Coffin, 1553
1	MS 0346	Ron Hopkins, 1553
1	MS 0346	Mike Ross, 1553
1	MS 0840	Jerry Rouse, 1553
1	MS 0483	Troy Savoie, 2224
1	MS 0613	Laura Jacobs, 2547
1	MS 1320	Denis Ridzal, 1441
1	MS 0845	Tim Walsh, 1542
1	MS 0897	Brett Clark, 1543
1	MS 0748	Mike Starr, 8853
1	MS 0386	Arup Maji , 1557
1	MS 0840	Troy Skousen, 1557
1	MS 0346	Jacque Moore, 1553
1	MS 0557	Dan Rohe, 1522
1	MS 0557	Bryan Witt, 1522
1	MS 0557	Brandon Zwink, 1522
1	MS 0897	Ted Blackert, 1543
1	MS 0840	Carl Sisemore, 1557
1	MS 0557	Vit Babuska, 1557
1	MS 0557	Garrett Nelson, 1557
1	MS 0557	Randy Mayes, 1522
1	MS 0899	Technical Library, 9536 (electronic copy)


Sandia National Laboratories